

1 Regulation of mitophagy by the NSL complex underlies 2 genetic risk for Parkinson's disease at 16q11.2 and MAPT

3 H1 loci

4 Marc P. M. Soutar,^{1,†} Daniela Melandri,^{1,†} Benjamin O'Callaghan,^{1,2,†} Emily Annuario,^{3,†}
5 Amy E. Monaghan,^{4,5} Natalie J. Welsh,^{2,6} Karishma D'Sa,^{2,7} Sebastian Guelfi,⁸ David
6 Zhang,^{1,2} Alan Pittman,⁹ Daniah Trabzuni,¹ Anouk H. A. Verboven,^{10,11} Kylie S. Pan,¹ Demis
7 A. Kia,^{1,2} Magda Bictash,^{4,5} Sonia Gandhi,^{1,2,7} Henry Houlden,¹ Mark R. Cookson,¹² Nael
8 Nadif Kasri,^{10,11} Nicholas W. Wood,^{1,2} Andrew B. Singleton,¹² John Hardy,^{1,2,5} Paul J.
9 Whiting,^{4,5} Cornelis Blauwendraat,¹² Alexander J. Whitworth,⁶ Claudia Manzoni,^{2,13} Mina
10 Ryten,^{2,8,‡} Patrick A. Lewis^{1,2,14,‡} and Hélène Plun-Favreau^{1,2,‡}

11
12 ^{†,‡}**These authors contributed equally to this work.**

13
14 1 UCL Queen Square Institute of Neurology, London, UK

15 2 Aligning Science Across Parkinson's (ASAP) Collaborative Research Network, Chevy
16 Chase, MD, 20815, USA

17 3 King's College, London, UK

18 4 UCL Alzheimer's Research UK, Drug Discovery Institute, London, UK

19 5 UCL Dementia Research Institute, London, UK

20 6 MRC Mitochondrial Biology Unit, University of Cambridge, Cambridge, UK

21 7 Francis Crick Institute, London, UK

22 8 UCL NIHR Great Ormond Street Hospital, London, UK

23 9 St Georges University, London, UK

1 10 Department of Human Genetics, Radboudumc, Donders Institute for Brain, Cognition, and
2 Behavior, 6500 HB Nijmegen, The Netherlands

3 11 Department of Cognitive Neuroscience, Radboudumc, Donders Institute for Brain,
4 Cognition and Behavior, 6500 HB Nijmegen, The Netherlands

5 12 Laboratory of Neurogenetics, National Institute on Aging, National Institutes of Health,
6 Bethesda, MD, USA

7 13 UCL School of Pharmacy, London, UK

8 14 Royal Veterinary College, London, UK

9

10 Correspondence to: Hélène Plun-Favreau

11 University College London Queen Square Institute of Neurology, Department of
12 Neurodegenerative Diseases, Queen Square House, Queen Square, London, WC1N 3BG

13 E-mail: h.plun-favreau@ucl.ac.uk

14

15 **Running Title:** New mitophagy Parkinson's risk genes

16

ACCEPTED MANUSCRIPT

1 ABSTRACT

2 Parkinson's disease is a common incurable neurodegenerative disease. The identification of
 3 genetic variants via genome-wide association studies has considerably advanced our
 4 understanding of the Parkinson's disease genetic risk. Understanding the functional
 5 significance of the risk loci is now a critical step towards translating these genetic advances
 6 into an enhanced biological understanding of the disease. Impaired mitophagy is a key
 7 causative pathway in familial Parkinson's disease, but its relevance to idiopathic Parkinson's
 8 disease is unclear. We used a mitophagy screening assay to evaluate the functional
 9 significance of risk genes identified through genome-wide association studies. We identified
 10 two new regulators of PINK1-dependent mitophagy initiation, KAT8 and KANSL1,
 11 previously shown to modulate lysine acetylation. These findings suggest PINK1-mitophagy
 12 is a contributing factor to idiopathic Parkinson's disease. *KANSL1* is located on chromosome
 13 17q21 where the risk associated gene has long been considered to be *MAPT*. While our data
 14 does not exclude a possible association between the *MAPT* gene and Parkinson's disease, it
 15 provides strong evidence that *KANSL1* plays a crucial role in the disease. Finally, these
 16 results enrich our understanding of physiological events regulating mitophagy and establish a
 17 novel pathway for drug targeting in neurodegeneration.

18 **Keywords:** GWAS; KANSL1; KAT8; mitophagy; Parkinson's disease

19 **Abbreviations:** ARA-C = Cytosine β -D-arabinofuranoside; ASE = Allele-Specific
 20 Expression; BRD4 = Bromodomain-containing protein 4; Cas = CRISPR associated protein;
 21 Coloc = Colocalization; CRISPR = Clustered Regularly Interspaced Short Palindromic
 22 Repeats; CRISPRi = CRISPR interference; dCas9 = enzymatically dead Cas9; DMEM =
 23 Dulbecco's Modified Eagle Medium; eQTL = Expression Quantitative Trait Loci; FBS =
 24 Foetal Bovine Serum; FDR = False Discovery Rate; GTEX = Genotype-Tissue Expression;
 25 GWAS = Genome-Wide Association Study; HBSS = Hanks' Balanced Salt Solution; HCFC1
 26 = Host Cell Factor C1; HCS = High Content Screen; hiPSC = Human Induced Pluripotent
 27 Stem Cell; IB = Immunoblot; IF = Immunofluorescence; IMEX = International Molecular
 28 Exchange; KANSL1 = KAT8 Regulatory NSL Complex Subunit 1; KANSL2 = KAT8
 29 Regulatory NSL Complex Subunit 2; KANSL3 = KAT8 Regulatory NSL Complex Subunit
 30 3; KAT = Lysine Acetyltransferase; KAT8 = Lysine Acetyltransferase 8; KD = Knockdown;
 31 LD = Linkage Disequilibrium; LoF = Loss of Function; MCRS1 = Microspherule Protein 1;
 32 Ψ_m = Mitochondrial Membrane Potential; MSL = Male-Specific Lethal; NA = Numerical
 33 Aperture; NEAAs = Non-Essential Amino Acids; No TD = No Transduction; NSL = Non-
 34 Specific Lethal; O/A = Oligomycin/Antimycin; OGT = O-linked N-

1 acetylglucosaminyltransferase; ORFs = Open Reading Frames; PBS = Phosphate Buffered
2 Saline; PD = Parkinson's Disease; PFA = Para-Formaldehyde; PHF20 = PHD Finger Protein
3 20; PINK1 = PTEN-induced kinase 1; POE = Parkin Overexpressing; pParkin(Ser65) =
4 Phosphorylated Parkin (Serine65); PPI = Protein-Protein Interaction; pRab8A(Ser111) =
5 Phosphorylated Rab8a (Serine111); pUb(Ser65) = Phosphorylated Ubiquitin (Serine 65);
6 ROCKi = Rho Kinase Inhibitor; SCR = Scrambled; SD = Standard Deviation; sgRNA =
7 Single Guide RNA; siRNA = Small Interfering RNA; SNPs = Single Nucleotide
8 Polymorphisms; TET-ON = Tetracycline-ON; TMRM = Tetramethylrhodamine, Methyl
9 Ester, Perchlorate; TWAS = Transcriptome-Wide Association Analysis; WDR5 = WD
10 Repeat Domain 5; WPPINA = Weighted Protein-Protein Interaction Network Analysis

11
12

ACCEPTED MANUSCRIPT

1 INTRODUCTION

2 Parkinson's disease (PD) is the most common movement disorder of old age and
3 afflicts more than 125,000 in the UK ¹. Temporary symptomatic relief remains the
4 cornerstone of current treatments, with no disease-modifying therapies yet available ². Until
5 recently, the genetic basis for PD was limited to family-based linkage studies, favouring the
6 identification of rare Mendelian genes of high penetrance and effect. However, genome-wide
7 association studies (GWAS) have identified large numbers of common genetic variants
8 linked to increased risk of developing the disease ^{3,4}. While these genetic discoveries have led
9 to a rapid improvement in our understanding of the genetic architecture of PD ⁵, they have
10 resulted in two major challenges for the research community. First, conclusively identifying
11 the causal gene(s) for a given risk locus, and secondly dissecting their contribution to disease
12 pathogenesis. Addressing these challenges is critical for moving beyond genetic insights to
13 developing new disease-modifying strategies for PD.

14 Previous functional analyses of *PINK1* and *PRKN*, two genes associated with
15 autosomal recessive PD, have highlighted the selective degradation of damaged mitochondria
16 (mitophagy) as a key contributor to disease pathogenesis. In mammalian cells, the
17 mitochondrial kinase PINK1 selectively accumulates at the surface of damaged mitochondria,
18 where it phosphorylates ubiquitin, leading to the recruitment and phosphorylation of the E3
19 ubiquitin ligase Parkin. The recruitment of autophagy receptors leads to the engulfment of
20 damaged mitochondria in autophagosomes, and ultimately fusion with lysosomes ⁶⁻¹¹. It has
21 subsequently become clear that other PD-associated Mendelian genes, such as *FBXO7*, *DJ-1*
22 and *VPS35* ¹², are implicated in the regulation of PINK1-mediated mitochondrial quality
23 control. Based upon these data, we hypothesised that PD-GWAS candidate genes may also be
24 involved in this process, providing a mechanistic link between these genes and the aetiology
25 of idiopathic PD. In order to test that hypothesis, we used functional genomics to prioritise
26 candidate genes at the PD GWAS loci, and we developed a phenotypic high content
27 screening assay as a tool to identify genes that regulate PINK1-dependent mitophagy
28 initiation, and as such, are likely to be genes that influence the risk of developing PD.

29 In this study, we show that PD GWAS risk gene candidates KAT8 and KANSL1, that
30 are both part of the non-specific lethal (NSL) complex, are new and important regulators of
31 PINK1-mediated mitochondrial quality control. KAT8 is a histone acetyltransferase
32 belonging to the MYST family that represents the major catalytic constituent of two distinct
33 protein complexes: the male-specific lethal (MSL) and NSL complex ^{13,14}. Alongside KAT8,

1 the NSL complex consists of 8 additional proteins HCFC1, KANSL1, KANSL2, KANSL3,
2 MCRS1, OGT, PHF20, WDR5¹³. KAT8 is the catalytically active acetyltransferase of the
3 NSL complex, responsible for the deposition of acetylation modifications on lysine 16 of
4 histone H4 (H4K16ac) facilitating chromatin decompaction making it more permissible for
5 transcriptional machinery and target gene expression¹⁵, in addition to protranscriptional
6 H4K5ac and H4K8ac¹⁶. The NSL complex regulates the expression of genes involved in a
7 multitude of crucial biological processes including proliferation, metabolism, transcription,
8 DNA replication and autophagy¹⁵⁻²³. In addition to its canonical role in the nucleus,
9 components of the NSL complex have also been suggested to partially localise to the
10 mitochondria (KAT8, KANSL1, KANSL2, KANSL3 and MCRS1) where they regulate
11 mtDNA transcription and mitochondrial oxidative metabolism²⁴.

12 These findings suggest that mitophagy contributes to idiopathic PD and provides a
13 proof of principle for functional screening approaches to identify causative genes in GWAS
14 loci. Finally, these results suggest lysine acetylation as a potential new avenue for mitophagy
15 modulation and therapeutic intervention.

16

17 **MATERIALS AND METHODS**

18 The following methods are available on protocols.io: Cell-Based in vitro Assays,
19 [dx.doi.org/10.17504/protocols.io.5jyl89648v2w/v1](https://doi.org/10.17504/protocols.io.5jyl89648v2w/v1); Bioinformatic Prioritisation and Hit
20 Validation, [dx.doi.org/10.17504/protocols.io.3byl4br2zvo5/v1](https://doi.org/10.17504/protocols.io.3byl4br2zvo5/v1); Drosophila stocks,
21 husbandry, locomotor and lifespan assays, and immunohistochemistry and sample
22 preparation, [dx.doi.org/10.17504/protocols.io.eq2lyn1dqvx9/v1](https://doi.org/10.17504/protocols.io.eq2lyn1dqvx9/v1).

23

24 **Reagents**

25 Oligomycin (mitochondrial complex V inhibitor) was purchased from Cayman Chemicals
26 (11341) and from Sigma-Aldrich (O4876), and antimycin A (mitochondrial complex III
27 inhibitor) were purchased from Sigma-Aldrich (A8674). All siRNAs were purchased as pre-
28 designed siGENOME SMARTpools from Dharmacon: non-targeting (D-001206-13), PINK1
29 (M-004030-02), PLK1 (L-003290-00), KIF-11 (L-003317-00), KAT8 (M-014800-00),
30 KANSL1 (M-031748-00), KANSL2 (M-020816-01), KANSL3 (M-016928-01), HCFC1 (M-
31 019953-01), MCRS1 (M-018557-00), OGT (M-019111-00), PHF20 (M-015234-02), WDR5

1 (M-013383-01). The following antibodies were used for immunocytochemistry: mouse anti
2 TOM20 (Santa Cruz, sc-17764, RRID:AB_628381, 1:1000), rabbit anti phospho-ubiquitin
3 (Ser65) (Cell Signaling, 37642, 1:1000), rabbit anti phospho-Parkin (Ser65) (Abcam/Michael
4 J. Fox Foundation, MJF17, 1:250), rabbit anti FLAG (Sigma-Aldrich, F7425,
5 RRID:AB_439687, 1:500), AlexaFluor 488 goat anti rabbit (Invitrogen, A11008,
6 RRID:AB_143165, 1:2000), AlexaFluor 568 goat anti mouse (Invitrogen, A11004,
7 RRID:AB_2534072, 1:2000), AlexaFluor 488 donkey anti-rabbit (Invitrogen, A21206,
8 RRID:AB_2535792, 1:2000), AlexaFluor 647 donkey anti-mouse (Invitrogen, A31571,
9 RRID:AB_162542, 1:2000). The following antibodies were used for immunoblotting: mouse
10 anti TIM23 (BD Biosciences, 611223, RRID:AB_398755, 1:1000), rabbit anti TOM20
11 (Santa Cruz, sc-11415, RRID:AB_2207533, 1:1000), rabbit anti phospho-ubiquitin (Ser65)
12 (Merck Millipore, ABS1513-I, RRID:AB_2858191, 1:1000; and Cell Signaling, 37642,
13 1:1000), mouse anti GAPDH (Abcam, ab110305, RRID:AB_10861081, 1:10000), rabbit anti
14 KAT8 (Abcam, ab200660, RRID:AB_2891127, 1:1000), rabbit anti total-Tau (DAKO,
15 A0024, RRID:AB_10013724, 1:10000), mouse anti V5 tag (Invitrogen, R960-25,
16 RRID:AB_2556564, 1:1000), rabbit anti KANSL1 (Sigma-Aldrich, HPA006874,
17 RRID:AB_1852393, 1:500), rabbit anti pParkin(Ser65) (Abcam/Michael J. Fox Foundation,
18 MJF17, 1:1000), mouse anti FLAG M2 (Sigma-Aldrich, F3165, RRID:AB_259529, 1:1000),
19 sheep anti pRab8A(Ser111) (MRC Protein Phosphorylation and Ubiquitylation Unit,
20 University of Dundee, 1ug/ml preblocked with 10ug/ml non-phosphorylated peptide ²⁵),
21 rabbit anti total Rab8 (Cell Signaling, 6975, RRID:AB_10827742, 1:1000), IRDye 680LT
22 donkey anti mouse (LI-COR Biosciences, 925-68022, RRID:AB_2814906, 1:20000), IRDye
23 800CW donkey anti rabbit (LI-COR Biosciences, 925-32213, RRID:AB_2715510, 1:20000),
24 IRDye 800CW Donkey anti-Goat (LI-COR Biosciences, 926-32214, RRID:AB_621846,
25 1:20000), IRDye® 680RD Goat anti-Rabbit (LI-COR Biosciences, 926-68071,
26 RRID:AB_10956166, 1:20000). The generation of rabbit monoclonal anti PINK1 antibody
27 has been described elsewhere ²⁶, and is available on reasonable request to the corresponding
28 author.

29

30 **Selection of genes for High Content Screening**

31 Candidates for High Content Screening were selected based on i) Weighted Protein-Protein
32 Interaction Network Analysis (WPPINA); ii) complex prioritization; and, iii) coloc analysis.

1 WPPINA analysis is reported in ²⁷ where the 2014 PD GWAS ²⁸ was analysed; candidate
2 genes were selected among those prioritised and with a linkage disequilibrium (LD)
3 $r^2 \geq 0.8$. The same pipeline has then been additionally applied to the 2017 PD GWAS ³ to
4 update the list of candidate genes. Briefly, a protein-protein interaction network has been
5 created based on the Mendelian genes for PD (seeds) using data from databases within the
6 IMEx consortium. The network has been topologically analysed to extract the core network
7 (i.e. the most interconnected part of the network). The core network contains the
8 proteins/genes that can connect >60% of the initial seeds and are therefore considered
9 relevant for sustaining communal processes and pathways, shared by the seeds. These
10 processes have been evaluated by Gene Ontology Biological Processes enrichment analysis.
11 The top single nucleotide polymorphisms (SNPs) of the 2017 PD GWAS have been used to
12 extract open reading frames (ORFs) in cis-haplotypes defined by LD $r^2 \geq 0.8$ (analysis
13 performed in October 2017). These ORFs have been matched to the core network to identify
14 overlapping proteins/genes in relevant/shared pathways. Results of complex prioritization
15 (neurocentric prioritization strategy) were gathered from ³ where this strategy was applied to
16 the 2017 PD GWAS. The coloc analysis was performed as reported in ²⁹, posterior
17 probabilities for the hypothesis that both traits, the regulation of expression of a given gene
18 and the risk for PD share a causal variant (PPH4), were calculated for each gene, and genes
19 with $PPH4 \geq 0.75$ were considered to have strong evidence for colocalization. Summary
20 statistics were obtained from the most recent PD GWAS ⁴ and were used for regional
21 association plotting using LocusZoom ³⁰. With the exception of *PM20D1* all genes are
22 expressed in SHSY5Y cells according to publically available expression data deposited in the
23 Human Protein Atlas (proteatlas.org) ³¹ and EBI Expression Atlas
24 (<http://www.ebi.ac.uk/gxa>) ³².

25

26 **Cell Culture and siRNA transfection**

27 Parkin over-expressing (POE) SHSY5Y cells are a kind gift from H. Ardley ³³ and the mt-
28 Keima POE SHSY5Y cells were a kind gift of C. Luft ³⁴. PINK1-HA overexpressing
29 SHSY5Y cells were a kind gift from E. Deas ³⁵. WT SHSY5Y (RRID:CVCL_0019) and H4
30 (RRID:CVCL_1239) cells were sourced from American Type Culture Collection (ATCC,
31 RRID:SCR_00167). Lenti-X 293T human embryonic kidney (HEK) cells were sourced from
32 Takara Bio (632180, RRID: CVCL_4401). Cells were cultured in Dulbecco's Modified Eagle
33 Medium (DMEM, Gibco, 11995-065) supplemented with 10% heat-inactivated foetal bovine

1 serum (FBS, Gibco) in a humidified chamber at 37 °C with 5% CO₂. For siRNA transfection,
2 cells were transfected using DharmaFECT1 transfection reagent (Dharmacon, T-2001-03)
3 according to the manufacturer's instructions (for concentrations of siRNA, see sections
4 below). Whole genome-sequencing shows SHSY5Ys are of the H1/H1 haplotype (data not
5 shown).

8 **KANSL1 iNeuron Culture and Differentiation**

9 Isogenic human induced pluripotent stem cell (hiPSC) lines with/without a heterozygous loss
10 of function (LoF) frameshift mutation in Exon2 of the KANSL1 gene (c.531insT), which
11 have also being stable transduced with transgenes permitting doxycycline-inducible
12 overexpression of murine Ngn2 were a kind gift from the lab of N. Nadif Kasri and have
13 been published elsewhere²². Whole genome-sequencing shows the parental line is of the
14 H1/H2 haplotype, with Sanger sequencing of KANSL1 cDNA revealing the LoF frameshift
15 mutation in the KANSL1^{+/-} line is on the H2 haplotype (i.e. H1/-) (data not shown). hiPSCs
16 were cultured on Geltrex (Thermofisher) coated culture dishes in mTeSR1 (StemCell
17 Technologies) and maintained in a humidified 37 °C incubator, 5% CO₂.

18 Isogenic KANSL1^{+/+} and KANSL1^{+/-} hiPSCs were differentiated into excitatory cortical
19 neurons by doxycycline induced overexpression of murine Ngn2 by adapting recently
20 published protocols^{22,36}. On d0 hiPSCs were first dissociated into a single cell suspension
21 using accutase (Sigma) before plating in induction medium consisting of DMEM/F12
22 supplemented with 1x Glutamax, 1x non-essential amino acids (NEAAs), 1x N2-supplement
23 (all Thermofisher), 4 µg/ml doxycycline (Sigma). Induction media was additionally
24 supplemented with 10 µM Y-27632 Rho Kinase inhibitor (ROCKi, Peprotech) during initial
25 seeding. 7.5x10⁵ cells were seeded onto geltrex coated 6-well plates. 24 h later (d1) and 48
26 h later (d2) a full medium change was performed with freshly prepared induction media
27 without Y-27632 ROCKi. On d3 a full medium change was performed with freshly prepared
28 N2-B27 media consisting of a 1:1 mixture of DMEM/F12:Neurobasal supplemented with
29 0.5x N2-supplement, 0.5x B27 supplement, 0.5x NEAAs, 0.5x Glutamax, 45 µM 2-
30 Mercaptoethanol (all Thermofisher), 2.7 µg/ml insulin (Sigma). N2-B27 media was
31 additionally supplemented with 2 µM Cytosine β-D-arabinofuranoside (ARA-C) (Sigma) on
32 d3. A half media change with N2-B27 lacking ARA-C was performed every 3-4 days

1 thereafter. A half media change with N2-B27 was performed on d16 with cells collected for
2 experimental assays 24 h later on d17.

3

4 **CRISPRi-i3N iNeuron Culture and Differentiation**

5 A hiPSC line stably transduced with transgenes permitting doxycycline-inducible
6 overexpression of murine Ngn2 at the AAVS1 safe-harbor locus, and stably transduced with
7 constitutively expressed enzymatically dead Cas9 (dCas9)-KRAB transcriptional repressor
8 fusion protein at the CLYBL promoter safe-harbor locus (CRISPRi-i3N hiPSCs) was a kind
9 gift from the labs of M. E. Ward and M. Kampmann, and have been published elsewhere^{37,38}.
10 hiPSCs were cultured as outlined above for KANSL1 hiPSCs.

11 CRISPRi-i3N hiPSCs were first transduced with lentiviral particles encoding a mCherry-
12 reporter and sgRNA sequences targeting the promoter regions of *KANSL1*, *KAT8* or *PINK1*,
13 or a non-targeting sgRNA control (see Supplementary Table 1 for sgRNA sequences, and
14 below for lentiviral production). Transduced cells were then differentiated into excitatory
15 cortical neurons by doxycycline induced overexpression of Ngn2 by adapting recently
16 published protocols^{37,38}.

17 On d-1 CRISPRi-i3N hiPSCs were first dissociated into a single cell suspension using
18 accutase and reverse transduced with sgRNA lentiviral supernatant in mTeSR1 supplemented
19 with 5ug/ml polybrene and 10 μ M Y-27632 ROCKi. 4.5×10^5 cells were seeded onto
20 Geltrex-coated 6-well plates. 24 h later (d0) media was changed to induction media
21 (composition outlined above for KANSL1 iNeurons). 24 h later (d1) and 48 h later (d2) a full
22 medium change was performed with freshly prepared induction media. On d3, differentiating
23 iNeurons were dissociated into a single cell suspension using accutase (Sigma) and seeded in
24 N2-B27 media (composition outlined above for KANSL1 iNeurons) into Geltrex-coated 96-
25 well CellCarrier Ultra plates for immunofluorescence (IF) (3×10^4 cells per well) and 12-
26 well plates (5×10^5 cells per well) for biochemistry purposes. A half media change with N2-
27 B27 was performed the following day (d4) and every 3-4 days thereafter. A half media
28 change with N2-B27 was performed on d16 with cells collected for experimental assays 24 h
29 later on d17.

30

31

1 **Lentiviral Particle Generation**

2 70-90% confluent Lenti-X 293T HEK cells cultured in DMEM 10% FBS media were
3 transfected with pMD2.G and pCMVR8.74 alongside appropriate delivery plasmids:
4 pLV[Exp]-U6>sgRNA-hPGK>mApple (Vectorbuilder) plasmids (for sgRNA), empty
5 pLVX-EF1 α -IRES-Puro (Clontech, Takara Bio, 631988), V5-KANSL1 pLVX-EF1 α -IRES-
6 Puro, or V5-KAT8 pLV[Exp]-EF1 α -IRES-Puro at a 1:1:2 molar mass ratio using
7 Lipofectamine 3000 (Invitrogen). The next day a full media change was performed with
8 mTeSR1 (for sgRNA lentivirus) or DMEM 10% FBS media and cells cultured for 24 h. The
9 lentivirus containing mTeSR1 / DMEM 10% FBS was collected and diluted 1:2 with fresh
10 mTeSR1 or 10% FBS before filtering through 0.44 μ m PES filters. pMD2.G (Addgene
11 plasmid #12259, RRID:Addgene_12259) and pCMVR8.74 (Addgene plasmid #22036,
12 RRID:Addgene_22036) were gifts from Didier Trono. KANSL1 cDNA
13 (ENST00000432791.7) with N-terminal V5 tag was cloned into the pLVX-EF1 α -IRES-Puro
14 plasmid using SpeI and NotI restriction sites (doi:10.5281/zenodo.6903553). See
15 Supplementary Table 1 for sgRNA plasmids and V5-KAT8 pLV[Exp]-EF1 α -IRES-Puro
16 plasmids (Vectorbuilder).

18 **ASEs**

19 Sites of allele-specific expression (ASE) were identified as described by Guelfi and
20 colleagues³⁹ by mapping RNA-seq data to personalised genomes, an approach specifically
21 chosen because it aims to minimise the impact of mapping biases. RNA-seq data generated
22 from 49 putamen and 35 substantia nigra tissue samples from the UK Brain Expression
23 Consortium was used for this analysis³⁹ and can be accessed through European Genome-
24 phenome Archive numbers EGAS00001002113 and EGAS00001003065. All samples were
25 obtained from neuropathologically normal individuals of European descent and sites with
26 greater than 15 reads in a sample were tested for ASE. Only sites present in non-overlapping
27 genes were considered and data from both the tissues were considered together to increase
28 power. Sites with minimum false discovery rate (FDR) < 5% across samples were marked as
29 ASE sites. Plots were generated using Gviz3 (<https://bioconductor.org/packages/Gviz/>),
30 with gene and transcript details obtained from Ensembl v92 (<http://www.ensembl.org/>,
31 RRID:SCR_002344).

32

1 **High Content siRNA Screen**

2 *Cell plating and siRNA transfection*

3 siRNA was dispensed into Geltrex-coated 96-well CellCarrier Ultra plates (Perkin Elmer) at
4 a final concentration of 30 nM using the Echo 555 acoustic liquid handler (Labcyte). For
5 each well, 25 μ l of DMEM containing 4.8 μ l/ml of DharmaFECT1 transfection reagent was
6 added and incubated for 30 min before POE SHSY5Y cells were seeded using the CyBio
7 SELMA (Analytik Jena) at 15,000 cells per well, 100 μ l per well in DMEM + 10% FBS.
8 Cells were incubated for 72 h before treatment with 10 μ M oligomycin/10 μ M antimycin for
9 3 h to induce mitophagy. Positive hits from the screen were validated further, however
10 without determining functional siRNA KD of all gene targets in the screens, none of the
11 negative hits can be formally excluded as regulators of PINK1-dependent mitophagy
12 initiation.

13 *IF and Image Capture and Analysis*

14 Cells were fixed with 4% PFA (Sigma-Aldrich, F8775), then blocked and permeabilised with
15 10% FBS, 0.25% Triton X-100 in PBS for 1 h, before immunostaining with pUb(Ser65) and
16 TOM20 primary antibodies (in 10% FBS/PBS) for 2 h at room temperature. After 3x PBS
17 washes, AlexaFluor 568 anti-mouse and 488 anti-rabbit secondary antibodies and Hoechst
18 33342 (Thermo Scientific, 62249) were added (in 10% FBS/PBS, 1:2000 dilution for all) and
19 incubated for 1 h at room temperature. Following a final 3x PBS washes, plates were imaged
20 using the Opera Phenix (Perkin Elmer). 5x fields of view and 4x 1 μ m Z-planes were
21 acquired per well, using the 40X water objective, NA1.1. Images were analysed in an
22 automated way using the Columbus 2.8 analysis system (Perkin Elmer,
23 [https://www.perkinelmer.com/en-ca/product/image-data-storage-and-analysis-system-](https://www.perkinelmer.com/en-ca/product/image-data-storage-and-analysis-system-columbus)
24 [columbus](https://www.perkinelmer.com/en-ca/product/image-data-storage-and-analysis-system-columbus)) to measure the integrated intensity of pUb(Ser65) within the whole cell. First of
25 all, the image was loaded as a maximum projection, before being segmented to identify the
26 nuclei using the Hoechst 33342 channel (method B). The cytoplasm was then identified using
27 the “Find Cytoplasm” building block (method B) on the sum of the Hoechst and Alexa 568
28 channels. pUb(Ser65) was identified as spots (method B) on the Alexa 488 channel, before
29 measuring their integrated intensity.

30

1

2 ***Screen quality control, data processing and candidate selection***

3 Screen plates were quality controlled based on the efficacy of the PINK1 siRNA control and
4 O/A treatment window (minimum 3-fold). Data were checked for edge effects using
5 Dotmatics Vortex visualization software. Raw data was quality controlled using robust Z
6 prime > 0.5. Data were processed using Python (<http://www.python.org/>,
7 RRID:SCR_008394) for Z score calculation before visualization in Dotmatics Vortex.
8 Candidates were considered a hit where Z score was ≥ 2 or ≤ -2 , and where replication of
9 efficacy was seen both within and across plates.

10 ***siRNA libraries***

11 The siRNA libraries were purchased from Dharmacon as an ON-TARGETplus SMARTpool
12 Cherry-pick siRNA library, 0.25 nmol in a 384-well plate. siRNAs were resuspended in
13 RNase-free water for a final concentration of 20 μ M. SCR, PINK1 and PLK1 or KIF11
14 controls were added to the 384-well plate at a concentration of 20 μ M before dispensing into
15 barcoded assay-ready plates.

16

17 **Mitochondrial enrichment and Western blotting**

18 POE SHSY5Y and H4 cells were transfected with 100 nM siRNA and incubated for 72 h.
19 KANSL1 iNeurons were cultured as detailed above. Whole cell lysates were used from POE
20 SHSY5Y cells, H4 cells, and KANSL1 iNeurons. For some experiments, POE SHSY5Y
21 lysates were first fractionated into cytoplasmic and mitochondria-enriched preparations to
22 facilitate detection of mitochondrial localised proteins of interest. Samples were run on SDS-
23 PAGE before immunoblot (IB) with the Odyssey® CLx Imager (LI-COR Biosciences).
24 Mitochondrial enrichment and Western blotting protocols were described previously²⁶.

25

26 **siRNA KD Rescue**

27 POE SHSY5Ys were transfected with 25 nM siRNA (d0) and incubated for 48 h. siRNA KD
28 cells were then transduced with lentivirus in the presence of 10 μ g/ml polybrene (d2), full
29 media change performed the following day (d3) and collected 4 days post siRNA transfection
30 (and 2 days post lentivirus transduction) (d4).

1

2 **pRab8A(Ser111) Measurements**

3 SHSY5Y cells stably overexpressing PINK1-HA were transfected with 100 nM siRNA and
4 incubated for 72 h. 200 ug of protein (whole cell lysate) were immunoprecipitated with
5 Protein A Dynabeads™ (Invitrogen) prebound with 0.5 ug of rabbit anti total-Rab8 antibody
6 (Cell Signaling, 6975) at 4 °C overnight. Samples were eluted from the beads by heating at
7 95 °C in 2x LDS supplemented with 50mM DTT for 5min.

8

9 **Immunofluorescence**

10 SHSY5Y cells were reverse transfected with 50 nM siRNA in 96-well CellCarrier Ultra
11 plates according to the manufacturer's instructions and incubated for 72 h. CRISPRi-i3N
12 iNeurons were cultured as described above. Cells were then treated, fixed and stained as per
13 the screening protocol detailed above (for treatment concentrations and times, see
14 corresponding figures). For visualisation purposes, brightness and contrast settings were
15 selected on the SCR (siRNA KD SHSY5Y) or no transduction (No TD) (CRISPRi-i3N
16 iNeurons) controls and applied to all other images. Images are presented as maximum
17 projections of the channels for one field of view.

18

19 **RT-qPCR**

20 Total RNA was extracted from cells using the Monarch Total RNA Miniprep Kit (New
21 England Bioscience) with inclusion of the optional on-column DNase treatment and
22 quantified using a NanoDrop One Spectrophotometer (ThermoFisher Scientific). RNA was
23 then reverse transcribed in a 10 µl reaction with 2.5 U/µl SuperScript IV reverse transcriptase
24 with 2.5 µM random hexamers, 0.5 mM dNTPs, 5 mM DTT and 2 U/µl RNaseOUT (all
25 Invitrogen). Equal amounts of RNA were reverse transcribed for all samples of a single
26 experiment, with 500ng of RNA in a 10 µl reverse transcription reaction being the most
27 common. The cDNA product was then diluted such that 500ng of reverse transcribed RNA
28 would be in a 600 ul final volume (i.e. 0.83 ng/µl). 4 ul (i.e. 3.33 ng) of the diluted cDNA
29 was then subjected to quantitative real-time PCR (qPCR) using 1x Fast SYBR™ Green
30 Master Mix (Applied Biosystems) and 500 nM gene specific primer pairs (Supplementary
31 Table 2) on a QuantStudio™ 7 Flex Real-Time PCR System (Applied Biosystems). At least

1 2x technical replicates were performed for each sample and gene target combination, and a
2 RT⁻ control for all samples and gene target combinations was performed alongside in most
3 assays, with rare exceptions due to test well number limitations. Relative mRNA expression
4 levels were calculated using the $2^{-\Delta\Delta Ct}$ method and *RPL18A* (SHSY5Y and H4 cells) or *UBC*
5 (iNeurons) as the house-keeping gene.

7 **Mitophagy measurement using the mt-Keima reporter**

8 Stable mt-Keima expressing POE SHSY5Y cells were reverse transfected with 50 nM siRNA
9 in 96-well CellCarrier Ultra plates according to the manufacturer's instructions and incubated
10 for 72 h. For the assay, the cell medium was replaced with phenol-free DMEM + 10% FBS
11 containing Hoechst 33342 (1:10000) and either DMSO or 1 μ M oligomycin/1 μ M antimycin
12 to induce mitophagy. Cells were immediately imaged on the Opera Phenix (PerkinElmer) at
13 37 °C with 5% CO₂, acquiring 15x single plane fields of view, using the 63X water objective,
14 NA1.15. The following excitation wavelengths and emission filters were used: cytoplasmic
15 Keima: 488 nm, 650–760 nm; lysosomal Keima: 561 nm, 570–630 nm; Hoechst 33342: 375
16 nm, 435–480 nm. Images were analysed in an automated way using the Columbus 2.8
17 analysis system (Perkin Elmer) to measure the mitophagy index. Cells were identified using
18 the nuclear signal of the Hoechst 33342 channel, before segmenting and measuring the area
19 of the cytoplasmic and lysosomal mt-Keima. The mitophagy index was calculated as the ratio
20 between the total area of lysosomal mitochondria and the total area of mt-Keima (sum of the
21 cytoplasmic and lysosomal mtKeima areas) per well.

23 ***Drosophila* stocks and husbandry**

24 Flies were raised under standard conditions in a humidified, temperature-controlled incubator
25 with a 12h:12h light:dark cycle at 25°C, on food consisting of agar, cornmeal, molasses,
26 propionic acid and yeast. The following strains were obtained from the Bloomington
27 *Drosophila* Stock Center (RRID:SCR_006457): *mof* RNAi lines, P{TRiP.JF01701}
28 (RRID:BDSC_31401); and P{TRiP.HMS00537} (RRID:BDSC_58281); *nsII* RNAi lines,
29 P{TRiP.HMJ22458} (RRID:BDSC_58328); the pan-neuronal *nSyb-GAL4* driver
30 (RRID:BDSC_51941); and dopaminergic neuron driver (TH-GAL4; RRID:BDSC_8848);
31 and control (*lacZ*) RNAi P{GD936}v51446 (RRID:FlyBase_FBst0469426) from the Vienna

1 *Drosophila* Resource Center (RRID:SCR_013805). All experiments were conducted using
2 male flies.

3 ***Locomotor and lifespan assays***

4 The startle induced negative geotaxis (climbing) assay was performed using a counter-current
5 apparatus. Briefly, 20-23 males were placed into the first chamber, tapped to the bottom, and
6 given 10 s to climb a 10 cm distance. This procedure was repeated five times (five
7 chambers), and the number of flies that has remained into each chamber counted. The
8 weighted performance of several group of flies for each genotype was normalized to the
9 maximum possible score and expressed as *Climbing index*⁴⁰.

10 For lifespan experiments, flies were grown under identical conditions at low-density. Progeny
11 were collected under very light anaesthesia and kept in tubes of approximately 20 males each,
12 around 50-100 in total. Flies were transferred every 2-3 days to fresh medium and the number
13 of dead flies recorded. Percent survival was calculated at the end of the experiment after
14 correcting for any accidental loss.

15

16 ***Immunohistochemistry and sample preparation***

17 *Drosophila* brains were dissected from aged flies and immunostained as described previously
18 ⁴¹. Adult brains were dissected in PBS and fixed in 4% formaldehyde for 30 min on ice,
19 permeabilized in 0.3% Triton X-100 for 3 times 20 min, and blocked with 0.3% Triton X-100
20 plus 4% goat serum in PBS for 4 h at RT. Tissues were incubated with anti-tyrosine
21 hydroxylase (Immunostar Inc. #22491, RRID:AB_572268), diluted in 0.3% Triton X-100
22 plus 4% goat serum in PBS for 72 h at 4°C, then rinsed 3 times 20 min with 0.3% Triton X-
23 100 in PBS, and incubated with the appropriate fluorescent secondary antibodies overnight at
24 4°C. The tissues were washed 2 times in PBS and mounted on slides using Prolong Diamond
25 Antifade mounting medium (Thermo Fisher Scientific). Brains were imaged with a Zeiss
26 LMS 880 confocal. Tyrosine hydroxylase-positive neurons were counted under blinded
27 conditions.

28

29 ***Statistical Analysis***

30 Intensity measurements from imaging experiments were normalised for each experiment (see
31 figure legends and graphs). N numbers are shown in figure legends and refer to the number of

1 independent, replicate experiments. Within each experiment, the mean values of every
2 condition were calculated from a minimum of 3 technical replicates. Integrated density
3 measurements from Western blot experiments were normalised to control wells (see figure
4 legends and graphs). Wherever possible, normalisation to conditions for statistical
5 comparisons were avoided in order to maintain experimental error associated. GraphPad
6 Prism 9 (La Jolla, California, USA) was used for statistical analyses and graph production.
7 Data were subjected to either one-way or two-way ANOVA with Dunnett's post-hoc analysis
8 for multiple comparisons, unless otherwise stated. All error bars indicate mean \pm standard
9 deviation (SD) from replicate experiments.

10

11 **Data Availability**

12 Exome and genome variant data is available from Genome Aggregation Database (gnomAD):
13 <https://gnomad.broadinstitute.org/about> Version 2.1.1 and subsequent releases are available
14 for download: <https://gnomad.broadinstitute.org/downloads>, Google Cloud Public Datasets
15 (<https://cloud.google.com/public-datasets>), the Registry of Open Data on AWS
16 (<https://registry.opendata.aws/>), and Azure Open Datasets ([https://azure.microsoft.com/en-
17 us/services/open-datasets/](https://azure.microsoft.com/en-us/services/open-datasets/)).

18 Data sets from the IMEx consortium ⁴² (<https://www.imexconsortium.org/>) used for
19 WPPINA analysis data are reported by Ferrari et al. ²⁷: and available through
20 [doi:10.1186/s12864-018-4804-9](https://doi.org/10.1186/s12864-018-4804-9). 2014 PD GWAS data ²⁸ analysed is available through
21 [doi:10.1038/ng.3043](https://doi.org/10.1038/ng.3043). 2017 PD GWAS ³ data is available through [doi:10.1038/ng.3955](https://doi.org/10.1038/ng.3955). PD
22 GWAS summary statistics ⁴ are available through [doi:10.1016/S1474-4422\(19\)30320-5](https://doi.org/10.1016/S1474-4422(19)30320-5).

23 Genes expressed in SHSY5Y cells were accessed from expression data deposited in the
24 Human Protein Atlas (proteinatlas.org) and EBI Expression Atlas
25 (<https://www.ebi.ac.uk/gxa/home>).

26 Tabulated data for figures of the manuscript are available through
27 [doi:10.5281/zenodo.6952972](https://doi.org/10.5281/zenodo.6952972). The datasets generated, analysed, and reported in this
28 manuscript are available from the corresponding author on reasonable request.

29

30

31

1 **Software**

2 LocusZoom 30 (<http://locuszoom.org/>, RRID:SCR_021374) was used for the regional
3 association plotting of summary statistics from PD GWAS ⁴. Dotmatics Vortex v5.1 software
4 was used to check for edge effects and for visualisation
5 (<https://www.dotmatics.com/capabilities/vortex>). GraphPad Prism 9 (La Jolla, California,
6 USA) was used for statistical analyses and graph production: GraphPad Prism
7 (RRID:SCR_002798) (<https://www.graphpad.com/>).

8

9 **RESULTS**

10

11 **Bioinformatic prioritisation of PD GWAS candidates**

12 Genomic analyses of PD have identified over 80 loci associated with an increased lifetime
13 risk for disease ³. In contrast to Mendelian PD genes, however, the assignment of a causative
14 gene to a risk locus is often challenging. In order to identify new risk genes for PD, we
15 undertook a triage of PD GWAS candidate genes using a combination of methods: i)
16 Colocalization (Coloc) and transcriptome-wide association analysis (TWAS) ⁴³ using
17 expression quantitative trait loci (eQTLs) information derived from Braineac ⁴⁴, GTEx and
18 CommonMind resources ^{29,45} to link PD risk variants with specific genes, ii) weighted
19 protein-protein interaction (PPI) network analysis (WPPINA)²⁷ based on Mendelian genes
20 associated with PD, and iii) the prioritised gene set as described in PD-GWAS ^{3,28}. This
21 resulted in the nomination of 31 open reading frames (ORFs) as putatively causal for
22 associations at PD risk loci. 55% of these genes were prioritised through multiple techniques,
23 with three out of 31 genes (*KAT8*, *CTSB* and *NCKIPSD*) identified through all three
24 prioritization methods (Extended Data Fig. 1A). The 31 genes, together with 7 PD Mendelian
25 genes and lysosomal storage disorder genes, previously shown to be enriched for rare, likely
26 damaging variants in PD ⁴⁶, were then taken forward for functional analysis (Table 1).

27

28 **pUb(Ser65) based screen of prioritised genes identifies KAT8 as novel regulator of** 29 **PINK1-dependent mitophagy initiation.**

30 Based upon extensive data implicating impaired mitophagy in the aetiology of familial PD,
31 we hypothesized that PD-GWAS candidate genes, involved in the most common, idiopathic

1 form of the disease, may play a role in this process. In order to test whether the 38 prioritised
2 genes have a role in PINK1-mitophagy, we developed and optimized a high content
3 screening (HCS) assay for phosphorylation of ubiquitin at serine 65 (pUb(Ser65)), a PINK1-
4 dependent mitophagy initiation marker⁴⁷, following mitochondrial depolarization (Fig. 1A).
5 The 38 prioritised genes were individually knocked down (KD) using siRNA in Parkin over-
6 expressing (POE)-SHSY5Y human neuroblastoma cells. Increased mitochondrial clearance
7 following mitochondrial depolarization induced by treatment with 10 μ M of
8 oligomycin/antimycin A (O/A) was validated as an endpoint for mitophagy (Extended Data
9 Fig. 1B). Over 97% of the pUb(Ser65) signal colocalised with the TOM20 mitochondrial
10 marker in O/A treated cells (Extended Data Fig. 1C, D). KD efficiency was validated using
11 both a pool of *PINK1* siRNA, which decreased O/A induced pUb(Ser65) and subsequent
12 TOM20 degradation (Extended Data Fig. 1E-G) without decreasing cell viability (Extended
13 Data Fig. 2A-B), and a pool of Polo-like kinase 1 (PLK-1) siRNA that decreased cell
14 viability by apoptosis (Extended Data Fig. 2A-B). The siRNA pools for the 38 candidate
15 genes, together with controls, were screened in duplicate on each plate, across three replicate
16 plates per run. Hits were identified as those wells where O/A-induced pUb(Ser65) was
17 decreased or increased at greater than two standard deviations from the mean of the scramble
18 (SCR) negative control siRNA.

19 *KAT8* was selected based on reproducible downregulation of O/A-induced PINK1-
20 dependent pUb(Ser65) across all three replicates (Fig. 1B and Extended Data Fig. 1H),
21 without affecting cell viability (Extended Data Fig. 2C). Notably, *KAT8* was selected as a
22 candidate gene on the basis of all three prioritization criteria – namely, proximity of the lead
23 SNP to an ORF (Fig 1D), colocalization of a brain-derived eQTL signal with a PD GWAS
24 association signal (Extended Data Fig. 3) and evidence of PPI with a known PD gene (Table
25 1). Furthermore, we find that colocalization and TWAS⁴⁸ analyses at this locus are consistent
26 with the KD models in the HCS assay (Supplementary Tables 3 and 4)²⁹. Both methods
27 predict that the risk allele operates by reducing *KAT8* expression in PD cases versus controls.

28 The effect of *KAT8* KD on pUb(Ser65) was further validated in POE SHSY5Y cells
29 treated with 1 μ M O/A, using both immunoblotting (IB) and immunofluorescence (IF) (Fig.
30 1D-G and Extended Data Fig. 4). In order to assess whether other lysine acetyltransferases
31 (KATs) could regulate PINK1-dependent mitophagy, the pUb(Ser65) screen was repeated in
32 POE SHSY5Y cells silenced for 22 other KATs (Supplementary Table 5)^{49,50}. Only *KAT8*

1 KD led to a decreased pUb(Ser65) signal, emphasising the specificity of the KAT8 KD effect
2 on pUb(Ser65) (Fig. 1H).

3

4 **KANSL1, another NSL member and PD GWAS candidate, regulates PINK1-dependent** 5 **mitophagy and dopaminergic neuron viability**

6 These functional data complement and support the omic prioritization of *KAT8* as a causative
7 gene candidate for the chromosome 16q11.2 PD associated locus (Fig. 1C). To gain further
8 insight into a possible role for *KAT8* in the aetiology of PD, we explored the known
9 functional interactions of this protein.

10 KAT8 has previously been shown to partially localise to mitochondria as part of the
11 NSL complex together with *KANSL1*, *KANSL2*, *KANSL3*, and *MCRS1*²⁴. To test whether
12 other components of the NSL complex also modulate mitophagy, the pUb(Ser65) screen was
13 repeated in POE SHSY5Y cells silenced for each of the nine NSL components. Notably,
14 reduction of *KANSL1*, *KANSL2*, *KANSL3*, *MCRS1* and *KAT8* expression led to decreased
15 pUb(Ser65) after 1.5 or 3 h O/A treatment (Fig. 2A and Extended Data Fig. 5), suggesting
16 that the NSL complex modulates PINK1-dependent mitophagy initiation. Interestingly,
17 *KANSL1* is another PD GWAS candidate gene³. The effect of *KANSL1* KD on pUb(Ser65)
18 was further validated in POE SHSY5Y cells treated with 1 μ M O/A, using both IF and IB
19 (Fig. 2B-F).

20 Deconvolution of the individual siRNA within the respective pools (of 4x individual
21 siRNA against the target gene) (Extended Data Fig. 6) and rescue of the siRNA KD
22 phenotype with overexpression of V5-tagged *KANSL1*/*KAT8* (Extended Data Fig. 7) are
23 both supportive of on-target effect associated with *KANSL1*/*KAT8* KD. The effect of the
24 *KAT8* and *KANSL1* KD on pUb(Ser65) was confirmed in WT SHSY5Y cells and the
25 astrogloma H4 cell line, both of which are expressing endogenous levels of Parkin
26 (Extended Data Fig. 8). In order to further assess the effect of *KAT8* and *KANSL1* KD on
27 PINK1-dependent mitophagy initiation, we measured pUb(Ser65) levels over time (Fig. 3A-
28 B), as well as PINK1 recruitment (Fig. 1D and F, Fig. 2D and F), Parkin recruitment (Fig.
29 3C-D), PINK1-dependent phosphorylation of Parkin at Ser65 (pParkin(Ser65)) (Fig. 3E-F
30 and Extended Data Fig. 9)⁹, and PINK1-dependent (but indirect) phosphorylation of Rab8A
31 at Ser111 (pRab8A(Ser111))²⁵ (Extended Data Fig. 10). The reduction in pUb(Ser65) levels

1 is not associated with reduced availability of Parkin (Extended Data Fig. 9) or ubiquitin
2 (Extended Data Fig. 11).

3 Given the canonical function of the NSL complex as a pro-transcriptional epigenetic
4 remodelling complex^{15,16}, a strong candidate mechanism accounting for the reduced PINK1
5 protein accumulation and PINK1-dependant mitophagy initiation could be reduced *PINK1*
6 gene expression. In fact, RT-qPCR assessments of *PINK1* mRNA levels in WT and POE
7 SHSY5Ys, reveal that KANSL1 and to a lesser degree KAT8 KD, both reduce *PINK1* gene
8 expression (Fig. 4). These data are mirrored by both *PINK1* gene expression and PINK1
9 protein accumulation in H4 cells (Extended Data Fig. 8C,D,F-H). Finally, the reduction in
10 *PINK1* mRNA following KANSL1/KAT8 KD in POE SHSY5Ys is also rescued with
11 KANSL1/KAT8 overexpression (Extended Data Fig. 7C,D,G,H).

12 KD of both KAT8 and KANSL1 reduced subsequent mitochondrial clearance in live
13 POE-SHSY5Y cells, as measured by the mitophagy reporter mt-Keima⁵¹ (Fig. 5).

14 In order to assess the role of KAT8/KANSL1 in neuronal function and survival *in*
15 *vivo*, we used *Drosophila* as a model system. Notably, the NSL complex was originally
16 discovered in *Drosophila* through the homologs of *KAT8* and *KANSL1* (*mof* and *nsll*,
17 respectively), but null mutations for these genes are associated with developmental lethality
18 owing to profound transcriptional remodelling during development⁵². Therefore, we utilised
19 inducible transgenic RNAi strains to target the KD of *mof* and *nsll* specifically in neuronal
20 tissues. Using behavioural assays as a sensitive readout of neuronal function we found that
21 pan-neuronal KD of *mof* or *nsll* caused progressive loss of motor (climbing) ability
22 (Extended Data Fig. 12A, B), and also significantly shortened lifespan (Extended Data Fig.
23 12C, D). Interestingly, loss of *nsll* had a notably stronger effect than loss of *mof*. Consistent
24 with this, KD of *nsll* but not *mof*, in either all neurons or only in dopaminergic (DA)
25 neurons, caused the loss of DA neurons (Extended Data Fig. 12E, F).

26

27 **KANSL1 is a likely PD GWAS candidate at the 17q21 locus**

28 *KANSL1* is located within the extensively studied inversion polymorphism on chromosome
29 17q21 (Extended Data Fig. 13A, B), which also contains *MAPT* - a gene frequently
30 postulated to drive PD risk at this locus⁵³. While the majority of individuals inherit this
31 region in the direct orientation, up to 25% of individuals of European descent have a ~1mb
32 sequence in the opposite orientation^{54,55}, inducing a larger ~1.3–1.6 Mb region of linkage

1 disequilibrium (LD). Since this inversion polymorphism precludes recombination over a
2 region of ~1.3–1.6 Mb, haplotype-specific polymorphisms have arisen resulting in the
3 generation of two major haplotype clades, termed H1 (common haplotype) and H2 (inversion
4 carriers), with H1 previously strongly linked to neurodegenerative disease including PD^{56–58}.
5 Due to high LD, the genetics of this region have been hard to dissect, and robust eQTL
6 analyses have been challenging due to the issue of polymorphisms within probe sequences in
7 microarray-based analyses or mapping biases in RNA-seq-based analyses. Several variants
8 (rs34579536, rs35833914 and rs34043286) are in high LD with the H1/H2 haplotype and are
9 located within *KANSL1* (Fig. 6A,B), raising the possibility that they could directly impact on
10 *KANSL1* protein function. In particular, one of the variants is associated with a serine (H1
11 haplotype) or proline (H2 haplotype) amino acid change in *KANSL1* protein sequence
12 (NM_001193465:c.T2152C:p.S718P), and would therefore be predicted to alter the gross
13 secondary structure of the *KANSL1* protein (Fig. 6B). Furthermore, we explored the
14 possibility that PD risk might be mediated at this locus through an effect on *KANSL1*
15 expression. Using RNA sequencing data generated from 84 brain samples (substantia nigra
16 n=35; putamen n=49), for which we had access to whole exome sequencing and SNP
17 genotyping data thus enabling mapping to personalised genomes³⁹, we performed allele-
18 specific expression analysis. More specifically, we quantified the variation in expression
19 between the H1 and H2 haplotypes (Supplementary Table 8) amongst heterozygotes. While
20 we identified allele-specific expression sites within *MAPT* (Extended Data Fig. 14 and
21 Supplementary Table 9), we also identified 4 sites of allele-specific expression in *KANSL1*
22 (Fig. 6A), suggesting that the high PD risk H1 allele is associated with lower *KANSL1*
23 expression, consistent with our functional assessment. Interestingly, sequence analysis of the
24 human *KANSL1* haplotype revealed that the high risk H1 haplotype is the more recent
25 “mutant” specific to *Homo sapiens*, and that other primates and mammals share the rarer non-
26 risk ancestral H2 haplotype (Fig. 6B). To assess the specificity of the *KANSL1* KD effect on
27 PINK1-dependent mitophagy initiation, 32 open reading frames in linkage disequilibrium on
28 the H1 haplotype at the 17q21 locus (Extended data Fig. 13A, B and Supplementary Table
29 10) were knocked down individually and their effect on pUb(Ser65) was assessed. While the
30 effect of *KANSL1* KD on pUb(Ser65) was confirmed, neither the KD of *MAPT* (see also
31 Extended Data Fig. 15), nor the KD of each of the other 30 genes on this locus, led to a
32 decrease in the pUb(Ser65) signal (Fig. 6C). These data confirm the selectivity of our
33 mitophagy screening assay and suggest that *KANSL1* is likely to be a key PD risk gene at the
34 17q21 locus.

1
2
3
4
5
6
7
8
9
10
11
12
13
14
15
16
17
18
19
20
21
22
23
24
25
26
27
28
29
30
31
32

Impairments in PINK1-dependent mitophagy initiation are also observed in human iNeuron models of KANSL1 and KAT8 deficiency

Finally, we sought to validate the mitophagy initiation impairments associated with reductions in KANSL1 and KAT8, in more disease-relevant human induced pluripotent stem cell (hiPSC) derived neuron systems.

To this end, further experiments were performed using isogenic hiPSC lines with/without a heterozygous loss of function (LoF) frameshift mutation (c.531insT) in KANSL1 introduced through CRISPR/Cas technology²². These lines have also been stably transduced with transgenes conferring overexpression of murine neurogenin-2 (Ngn2) under a tetracycline-ON (TET-ON) system, permitting differentiation into human cortical neurons following doxycycline treatment (iNeurons). After 17 days in vitro (DIV), KANSL1 control (KANSL1^{+/+}) and heterozygous LoF (KANSL1^{+/-}) iNeurons with ~50% reduction in *KANSL1* gene expression (Extended Data Fig. 16A) were subjected to assessments of mitophagy initiation. Treatment of KANSL1^{+/+} iNeurons with 1 μ M O/A resulted in pUb(Ser65) deposition, which continued to increase across a prolonged 12 h treatment window (Fig. 7A, B). Whilst KANSL1^{+/-} iNeurons showed detectable pUb(Ser65) deposition, the levels were lower than that of the isogenic KANSL1^{+/+} iNeurons, with this difference being significant at 9 h and 12 h of O/A treatment (Fig. 7B).

Similar experiments were also performed using the CRISPRi-i3N iNeuron system which in addition to the presence of a TET-ON system for dox-induced Ngn2 mediated neuronal differentiation³⁷, also express an enzymatically dead Cas9 (dCas9)-KRAB transcriptional repressor fusion protein that permits target gene KD through introduction of sgRNA molecules for specific gene promoters³⁸. Similar to observations in the KANSL1^{+/-} iNeurons, and KANSL1/KAT8/PINK1 siRNA KD cell line models, CRISPRi KD of all three gene targets (Extended Data Fig. 16B-D) significantly reduced mitochondrial pUb(Ser65) following 9 h O/A treatment as assessed through IF (Fig. 7C, D).

These data support an important functional link between KANSL1, KAT8 and PINK1-dependent mitophagy initiation. While our data support reductions in *PINK1* gene expression as the most likely underlying mechanism for mitophagy impairment in KAT8 and KANSL1 deficient cell lines, further experiments will be required to determine whether KAT8/KANSL1-dependent *PINK1* gene expression regulation also explains mitophagy

1 impairments in other cellular and *in vivo* models, or/and whether other mechanisms could be
2 involved.

3

4 **DISCUSSION**

5 Since the first PD GWAS study was performed in 2006⁵⁹, GWAS have identified over 80
6 independent loci for PD⁴. However, translating GWAS findings into a new molecular
7 understanding of PD-associated pathways and new therapeutic targets has remained a major
8 challenge for the scientific community. In order to screen for PD GWAS candidate genes that play
9 a role in PINK1-mitophagy, and thus are likely to be genuine risk genes for PD, we have set up and
10 optimised a HCS for pUb(Ser65), a marker of PINK1-dependent mitophagy initiation, a key
11 pathway in PD pathogenesis. This approach allowed the successful identification of two new genes
12 associated with increased PD risk, that play a role in mitophagy. Interestingly, these two genes
13 were previously shown to be part of the same complex, the NSL complex.

14 This study demonstrates the substantial potential of functional screens to exploit genetic
15 data by providing orthogonal information that can confidently identify new risk genes. This is
16 particularly important in genomic regions with uniformly high linkage disequilibrium, such as the
17 17q21 inversion region which includes 32 ORFs of which many are highly expressed in brain and
18 where existing fine-mapping and functional genomic analyses have been inconclusive.
19 Interestingly, while *MAPT* has long been considered the risk associated gene at this locus, this has
20 recently been questioned by Dong and colleagues, who also raised the significance of *KANSL1* in
21 driving PD risk at the locus⁶⁰. In line with our data, eQTL analysis by other groups has shown the
22 PD risk H1 haplotype is associated with reduced *KANSL1* mRNA expression^{61,62}, and non-
23 synonymous H1 vs H2 haplotype *KANSL1* amino acid changes including K104T, N225D, S718P
24 and I1084 we describe in this manuscript have been confirmed to be in high linkage disequilibrium
25 through Sanger sequencing by another group⁶³. Similar to our data, eQTL analysis by others has
26 revealed that lower levels of *KAT8* gene expression are also linked to an increased PD risk³.

27 Furthermore, functional screening can simultaneously provide mechanistic insights as
28 exemplified in this case by the novel insights we provide into the molecular events regulating
29 mitochondrial quality control and which support a role for mitophagy as a contributing factor to
30 sporadic PD. *KANSL1* is part of the NSL complex and functions as a scaffolding protein by
31 binding other subunits, including *KAT8*¹⁴. Through the deposition of pro-transcriptional histone
32 acetylation marks, the NSL complex underscores an important regulator of target gene expression

1 ¹⁶. In this study we show that PINK1-dependent phosphorylation of ubiquitin is reduced in the
2 context of KANSL1 and KAT8 LoF and that this appears to be largely caused by a reduction in
3 *PINK1* gene expression, at least in the cell line models. We hypothesise that as a consequence of
4 reduced *PINK1* gene and PINK1 protein expression, mitochondrial accumulation of activated
5 PINK1 is reduced, leading to reduced pUb(Ser65) deposition, Parkin activation, and subsequent
6 mitochondrial clearance.

7 It was previously shown that depletion of KAT8/KANSL1 causes significant
8 downregulation of mitochondrial DNA transcription and translation, and ultimately impaired
9 mitochondrial respiration ²⁴. Future studies will need to determine whether KAT8/KANSL1-
10 dependent modulation of mitochondrial DNA or nuclear DNA encoded mitochondrial genes could
11 regulate PINK1 mitochondrial accumulation, activation and subsequent mitophagy. It has been
12 further proposed that the KAT8/KANSL1 complex has targets in the mitochondria other than the
13 mitochondrial DNA ²⁴. It will be interesting to determine whether the KAT8/KANSL1 complex
14 could acetylate ubiquitin, which has previously been shown to be acetylated on six out of its seven
15 lysines (K6, K11, K27, K33, K48, K63) ⁶⁴. It will also be interesting to understand further whether
16 the regulation of mitophagy related genes such as *PINK1*, is associated with a direct effect of the
17 NSL complex at target gene promoters, or as a consequence of other upstream biochemical
18 cascades, as previously described in the context of KANSL1 LoF ²².

19 KANSL1 haploinsufficiency caused by heterozygous pathogenic genetic variants in
20 KANSL1 is associated with the neurodevelopmental disorder Koolen-de Vries syndrome (KdVS;
21 OMIM #610443) ⁶⁵. Pathogenic variants in KAT8 have also been associated with developmental
22 disorders inclusive of a strong neurological phenotype ⁶⁶, underpinning the functional importance
23 of the NSL complex in neurodevelopment. Using iNeurons differentiated from KdVS-derived
24 patient hiPSCs and genome-edited KANSL1 heterozygous hiPSCs, we have recently shown that
25 KANSL1 deficiency leads to impairments in autophagic flux and lysosomal function which appear
26 to be largely caused by elevated cellular reactive oxygen species ²², and impairments in the
27 transcriptional regulation of autophagy related genes have also been described elsewhere in the
28 context of both KAT8 and KANSL1 LoF ^{20,23}. Together with our current work highlighting
29 *KANSL1* and *KAT8* as PD risk genes, these studies suggest that impairments in the autophagic
30 process could be a contributing pathomechanism for idiopathic disease. Alongside our own data
31 implicating impairments in PINK1-dependent mitophagy initiation, synergistic dysregulation in
32 autophagosome and lysosomal-dependent steps, downstream in the mitophagy process, highlight
33 clearance of damaged mitochondria as a particular vulnerability in the context of KAT8/KANSL1

1 LoF. While more severe KAT8/KANSL1 haploinsufficiency leads to impaired neurodevelopment,
2 more subtle changes in KAT8/KANSL1 and associated mitochondrial deficits, associated with
3 impaired bulk autophagy might lead to accumulation of cellular damage leading to selective
4 vulnerability of dopaminergic neurons later in life.

5 Our data highlight the utility of a cellular function high-content siRNA KD screen for
6 prioritisation of GWAS candidates, however it is important to be aware of limitations to the
7 use of such a strategy. While we have confirmed successful KD of KAT8 and KANSL1,
8 without evaluating KD of all genes screened (which can be challenging with high-throughput
9 screens), the potential pitfall for false-negatives remains. siRNA KD strategies are limited to
10 delineating the functional effect of reductions in the expression of a target gene, whereas
11 increased expression might be more disease and functionally relevant in some cases.

12 Important genetic discoveries in PD, in particular, the identification of the *PINK1*⁶⁷
13 and *PRKN* genes⁶⁸, opened the field of selective mitophagy⁷. However, there is still a clear
14 need for a better molecular understanding of mitochondrial quality control. Here we provide
15 new insights into the mechanism by identifying two new molecular players, KAT8 and
16 KANSL1. These new regulators of mitophagy provide the first direct evidence for a role of
17 the PINK1-mitophagy pathway in idiopathic PD and the convergence between familial and
18 idiopathic pathways in disease. Taken together, these findings open a novel avenue for the
19 therapeutic modulation of mitophagy in PD, with potential implications across drug
20 discovery in frontotemporal dementia and Alzheimer's disease, where mitophagy also plays
21 an important role in disease pathogenesis⁶⁹.

22

23 **ACKNOWLEDGEMENTS**

24 The authors would like to thank the Genome Aggregation Database (gnomAD) and the
25 groups that provided exome and genome variant data to these resources. A full list of
26 contributing groups can be found at <https://gnomad.broadinstitute.org/about>.

27

28 **FUNDING**

29 This work was supported in part by the UK Medical Research Council (MRC) funding to the
30 Dementia Platform UK (MR/M02492X/1), MRC core funding to the High-Content Biology
31 Platform at the MRC-UCL LMCB university unit (MC_U12266B) and MRC MBU

1 (MC_UU_00015/6), and by UCL Translational Research Office administered seed funds.
2 MS, EA, CM and DT are funded by MRC MR/N026004/1. DM is supported by an MRC
3 CASE studentship (MR/P016677/1). BO is supported by the Michael J. Fox Foundation for
4 Parkinson's Research (MJFF-010437). AM, MB and PW are funded by ARUK (ARUK-
5 2018DDI-UCL). MR was supported by the UK MRC through the award of Tenure-track
6 Clinician Scientist Fellowship (MR/N008324/1). This research was funded in whole or in
7 part by Aligning Science Across Parkinson's [Grant number: ASAP 000478] through the
8 Michael J. Fox Foundation for Parkinson's Research (MJFF). For the purpose of open access,
9 the author has applied a CC BY public copyright license to all Author Accepted Manuscripts
10 arising from this submission. This work was supported in part by the Intramural Research
11 Programs of the National Institute on Aging (NIA). We also acknowledge the support of the
12 NIHR BRC award to University College London Hospitals, UCL.

13

14 **COMPETING INTERESTS**

15 The authors declare that they have no conflict of interest

16

17 **SUPPLEMENTARY MATERIAL**

18 Supplementary material is available at *Brain* online.

19

1 REFERENCES

- 2 1. Hardy J, Lewis P, Revesz T, Lees A, Paisan-Ruiz C. The genetics of Parkinson's
3 syndromes: a critical review. *Curr Opin Genet Dev.* 2009;19(3):254-265.
4 doi:<https://doi.org/10.1016/j.gde.2009.03.008>
- 5 2. Connolly BS, Lang AE. Pharmacological Treatment of Parkinson Disease: A Review.
6 *JAMA.* 2014;311(16):1670-1683. doi:10.1001/jama.2014.3654
- 7 3. Chang D, Nalls MA, Hallgrímsson IB, et al. A meta-analysis of genome-wide
8 association studies identifies 17 new Parkinson's disease risk loci. *Nat Genet.*
9 2017;49(10):1511-1516. doi:10.1038/ng.3955
- 10 4. Nalls MA, Blauwendraat C, Vallerga CL, et al. Identification of novel risk loci, causal
11 insights, and heritable risk for Parkinson's disease: a meta-analysis of genome-wide
12 association studies. *Lancet Neurol.* 2019;18(12):1091-1102. doi:10.1016/S1474-
13 4422(19)30320-5
- 14 5. Nalls MA, Plagnol V, Hernandez DG, et al. Imputation of sequence variants for
15 identification of genetic risks for Parkinson's disease: a meta-analysis of genome-wide
16 association studies. *Lancet.* 2011;377(9766):641-649. doi:10.1016/S0140-
17 6736(10)62345-8
- 18 6. Narendra D, Tanaka A, Suen D-F, Youle RJ. Parkin is recruited selectively to impaired
19 mitochondria and promotes their autophagy. *J Cell Biol.* 2008;183(5):795-803.
20 doi:10.1083/jcb.200809125
- 21 7. McWilliams TG, Muqit MM. PINK1 and Parkin: emerging themes in mitochondrial
22 homeostasis. *Curr Opin Cell Biol.* 2017;45:83-91. doi:10.1016/j.ceb.2017.03.013
- 23 8. Narendra DP, Jin SM, Tanaka A, et al. PINK1 Is Selectively Stabilized on Impaired
24 Mitochondria to Activate Parkin. Green DR, ed. *PLoS Biol.* 2010;8(1):e1000298.
25 doi:10.1371/journal.pbio.1000298
- 26 9. Kazlauskaitė A, Kondapalli C, Gourlay R, et al. Parkin is activated by PINK1-
27 dependent phosphorylation of ubiquitin at Ser65. *Biochem J.* 2014;460(1):127-141.
28 doi:10.1042/BJ20140334
- 29 10. Shiba-Fukushima K, Arano T, Matsumoto G, et al. Phosphorylation of Mitochondrial
30 Polyubiquitin by PINK1 Promotes Parkin Mitochondrial Tethering. *PLoS Genet.*
31 2014;10(12). doi:10.1371/journal.pgen.1004861

- 1 11. Lazarou M, Sliter DA, Kane LA, et al. The ubiquitin kinase PINK1 recruits autophagy
2 receptors to induce mitophagy. *Nature*. 2015;524(7565):309-314.
3 doi:10.1038/nature14893
- 4 12. Plotegher N, Duchen MR. Crosstalk between lysosomes and mitochondria in
5 Parkinson's disease. *Front Cell Dev Biol*. 2017;5(DEC):2011-2018.
6 doi:10.3389/fcell.2017.00110
- 7 13. Cai Y, Jin J, Swanson SK, et al. Subunit Composition and Substrate Specificity of a
8 MOF-containing Histone Acetyltransferase Distinct from the Male-specific Lethal
9 (MSL) Complex. *J Biol Chem*. 2010;285(7):4268-4272.
10 doi:10.1074/JBC.C109.087981
- 11 14. Dias J, Van Nguyen N, Georgiev P, et al. Structural analysis of the
12 KANSL1/WDR5/KANSL2 complex reveals that WDR5 is required for efficient
13 assembly and chromatin targeting of the NSL complex. *Genes Dev*. 2014;28(9).
14 doi:10.1101/GAD.240200.114
- 15 15. Sheikh BN, Guhathakurta S, Akhtar A. The non-specific lethal (NSL) complex at the
16 crossroads of transcriptional control and cellular homeostasis . *EMBO Rep*.
17 2019;20(7). doi:10.15252/embr.201847630
- 18 16. Radzishenskaya A, Shliha P V., Grinev V V., et al. Complex-dependent histone
19 acetyltransferase activity of KAT8 determines its role in transcription and cellular
20 homeostasis. *Mol Cell*. 2021;81(8):1749-1765.e8.
21 doi:10.1016/J.MOLCEL.2021.02.012
- 22 17. Feller C, Prestel M, Hartmann H, Straub T, Söding J, Becker PB. The MOF-containing
23 NSL complex associates globally with housekeeping genes, but activates only a
24 defined subset. *Nucleic Acids Res*. 2012;40(4):1509-1522. doi:10.1093/NAR/GKR869
- 25 18. Ravens S, Fournier M, Ye T, et al. Mof-associated complexes have overlapping and
26 unique roles in regulating pluripotency in embryonic stem cells and during
27 differentiation. *Elife*. 2014;2014(3). doi:10.7554/ELIFE.02104.001
- 28 19. Gaub A, Sheikh BN, Basilicata MF, et al. Evolutionary conserved NSL
29 complex/BRD4 axis controls transcription activation via histone acetylation. *Nat*
30 *Commun* 2020 111. 2020;11(1):1-17. doi:10.1038/s41467-020-16103-0
- 31 20. Füllgrabe J, Lynch-Day MA, Heldring N, et al. The histone H4 lysine 16

- 1 acetyltransferase hMOF regulates the outcome of autophagy. *Nature*.
2 2013;500(7463):468-471.
- 3 21. Hale CM, Cheng Q, Ortuno D, et al. Identification of modulators of autophagic flux in
4 an image-based high content siRNA screen. *Autophagy*. 2016;12(4):713-726.
5 doi:10.1080/15548627.2016.1147669/SUPPL_FILE/KAUP_A_1147669_SM6249.ZIP
- 6 22. Linda K, Lewerissa EI, Verboven AHA, et al. Imbalanced autophagy causes synaptic
7 deficits in a human model for neurodevelopmental disorders. *Autophagy*. Published
8 online 2021.
9 doi:10.1080/15548627.2021.1936777/SUPPL_FILE/KAUP_A_1936777_SM2241.ZIP
- 10 23. Li T, Lu D, Yao C, et al. Kans11 haploinsufficiency impairs autophagosome-lysosome
11 fusion and links autophagic dysfunction with Koolen-de Vries syndrome in mice. *Nat*
12 *Commun* 2022 131. 2022;13(1):1-16. doi:10.1038/s41467-022-28613-0
- 13 24. Chatterjee A, Seyfferth J, Lucci J, et al. MOF Acetyl Transferase Regulates
14 Transcription and Respiration in Mitochondria. *Cell*. 2016;167(3):722-738.e23.
15 doi:10.1016/j.cell.2016.09.052
- 16 25. Lai Y-C, Kondapalli C, Lehneck R, et al. Phosphoproteomic screening identifies Rab
17 GTPases as novel downstream targets of PINK1. *EMBO J*. 2015;34(22):2840-2861.
18 doi:10.15252/EMBJ.201591593
- 19 26. Soutar MPM, Kempthorne L, Miyakawa S, et al. AKT signalling selectively regulates
20 PINK1 mitophagy in SHSY5Y cells and human iPSC-derived neurons. *Sci Rep*.
21 2018;8(1):8855. doi:10.1038/s41598-018-26949-6
- 22 27. Ferrari R, Kia DA, Tomkins JE, et al. Stratification of candidate genes for Parkinson's
23 disease using weighted protein-protein interaction network analysis. *BMC Genomics*.
24 2018;19(1):452. doi:10.1186/s12864-018-4804-9
- 25 28. Nalls MA, Pankratz N, Lill CM, et al. Large-scale meta-analysis of genome-wide
26 association data identifies six new risk loci for Parkinson's disease. *Nat Genet*.
27 2014;46(9):989-993. doi:10.1038/ng.3043
- 28 29. Kia DA, Zhang D, Guelfi S, et al. Integration of eQTL and Parkinson's disease GWAS
29 data implicates 11 disease genes. *bioRxiv*. Published online 2019:627216.
30 doi:10.1101/627216
- 31 30. Pruim RJ, Welch RP, Sanna S, et al. LocusZoom: regional visualization of genome-

- 1 wide association scan results. *Bioinformatics*. 2010;26(18):2336-2337.
2 doi:10.1093/bioinformatics/btq419
- 3 31. Marti-Solano M, Crilly SE, Malinverni D, et al. Combinatorial expression of GPCR
4 isoforms affects signalling and drug responses. *Nat* 2020 5877835.
5 2020;587(7835):650-656. doi:10.1038/s41586-020-2888-2
- 6 32. Papatheodorou I, Moreno P, Manning J, et al. Expression Atlas update: from tissues to
7 single cells. *Nucleic Acids Res*. 2020;48(D1):D77-D83. doi:10.1093/NAR/GKZ947
- 8 33. Ardley HC, Scott GB, Rose SA, Tan NGS, Markham AF, Robinson PA. Inhibition of
9 proteasomal activity causes inclusion formation in neuronal and non-neuronal cells
10 overexpressing Parkin. *Mol Biol Cell*. 2003;14(11):4541-4556. doi:10.1091/mbc.E03-
11 02-0078
- 12 34. Soutar MPM, Kempthorne L, Annuario E, et al. FBS/BSA media concentration
13 determines CCCP's ability to depolarize mitochondria and activate PINK1-PRKN
14 mitophagy. *Autophagy*. 2019;15(11):2002-2011. doi:10.1080/15548627.2019.1603549
- 15 35. Deas E, Plun-Favreau H, Gandhi S, et al. PINK1 cleavage at position A103 by the
16 mitochondrial protease PARL. *Hum Mol Genet*. 2011;20(5):867-879.
17 doi:10.1093/HMG/DDQ526
- 18 36. Frega M, van Gestel SHC, Linda K, et al. Rapid Neuronal Differentiation of Induced
19 Pluripotent Stem Cells for Measuring Network Activity on Micro-electrode Arrays. *J*
20 *Vis Exp*. 2017;(119):e54900. doi:10.3791/54900
- 21 37. Fernandopulle MS, Prestil R, Grunseich C, Wang C, Gan L, Ward ME. Transcription
22 Factor-Mediated Differentiation of Human iPSCs into Neurons. *Curr Protoc cell Biol*.
23 2018;79(1). doi:10.1002/CPCB.51
- 24 38. Tian R, Gachechiladze MA, Ludwig CH, et al. CRISPR interference-based platform
25 for multimodal genetic screens in human iPSC-derived neurons. *Neuron*.
26 2019;104(2):239. doi:10.1016/J.NEURON.2019.07.014
- 27 39. Guelfi S, D'Sa K, Botía JA, et al. Regulatory sites for splicing in human basal ganglia
28 are enriched for disease-relevant information. *Nat Commun* 2020 111. 2020;11(1):1-
29 16. doi:10.1038/s41467-020-14483-x
- 30 40. Greene JC, Whitworth AJ, Kuo I, Andrews LA, Feany MB, Pallanck LJ.
31 Mitochondrial pathology and apoptotic muscle degeneration in Drosophila

- 1 parkin; mutants. *Proc Natl Acad Sci.* 2003;100(7):4078 LP - 4083.
2 doi:10.1073/pnas.0737556100
- 3 41. Whitworth AJ, Theodore DA, Greene JC, Beneš H, Wes PD, Pallanck LJ. Increased
4 glutathione S-transferase activity rescues dopaminergic neuron
5 loss in a Drosophila model of Parkinson's disease. *Proc*
6 *Natl Acad Sci.* 2005;102(22):8024 LP - 8029. doi:10.1073/pnas.0501078102
- 7 42. Orchard S, Ammari M, Aranda B, et al. The MIntAct project—IntAct as a common
8 curation platform for 11 molecular interaction databases. *Nucleic Acids Res.*
9 2014;42(D1):D358-D363. doi:10.1093/NAR/GKT1115
- 10 43. Giambartolomei C, Vukcevic D, Schadt EE, et al. Bayesian Test for Colocalisation
11 between Pairs of Genetic Association Studies Using Summary Statistics. Williams
12 SM, ed. *PLoS Genet.* 2014;10(5):e1004383. doi:10.1371/journal.pgen.1004383
- 13 44. Ramasamy A, Trabzuni D, Guelfi S, et al. Genetic variability in the regulation of gene
14 expression in ten regions of the human brain. *Nat Neurosci.* 2014;17(10):1418-1428.
15 doi:10.1038/nn.3801
- 16 45. Lonsdale J, Thomas J, Salvatore M, et al. The Genotype-Tissue Expression (GTEx)
17 project. *Nat Genet.* 2013;45(6):580-585. doi:10.1038/ng.2653
- 18 46. Robak LA, Jansen IE, Van Rooij J, et al. Excessive burden of lysosomal storage
19 disorder gene variants in Parkinson's disease. *Brain.* 2017;140(12):3191-3203.
20 doi:10.1093/brain/awx285
- 21 47. Hou X, Fiesel FC, Truban D, et al. Age- and disease-dependent increase of the
22 mitophagy marker phospho-ubiquitin in normal aging and Lewy body disease.
23 *Autophagy.* 2018;14(8):1404-1418. doi:10.1080/15548627.2018.1461294
- 24 48. Gusev A, Ko A, Shi H, et al. Integrative approaches for large-scale transcriptome-wide
25 association studies. *Nat Genet.* 2016;48(3):245-252. doi:10.1038/ng.3506
- 26 49. Simon RP, Robaa D, Alhalabi Z, Sippl W, Jung M. KATching-Up on Small Molecule
27 Modulators of Lysine Acetyltransferases. *J Med Chem.* 2016;59(4):1249-1270.
28 doi:10.1021/acs.jmedchem.5b01502
- 29 50. Sheikh BN, Akhtar A. The many lives of KATs — detectors, integrators and
30 modulators of the cellular environment. *Nat Rev Genet.* 2019;20(January).
31 doi:10.1038/s41576-018-0072-4

- 1 51. Katayama H, Kogure T, Mizushima N, Yoshimori T, Miyawaki A. A sensitive and
2 quantitative technique for detecting autophagic events based on lysosomal delivery.
3 *Chem Biol.* 2011;18(8):1042-1052. doi:10.1016/j.chembiol.2011.05.013
- 4 52. Raja SJ, Charapitsa I, Conrad T, et al. The Nonspecific Lethal Complex Is a
5 Transcriptional Regulator in *Drosophila*. *Mol Cell.* 2010;38(6):827-841.
6 doi:10.1016/j.molcel.2010.05.021
- 7 53. Wray S, Lewis PA. A tangled web - tau and sporadic Parkinson's disease. *Front*
8 *Psychiatry.* 2010;1(DEC):1-7. doi:10.3389/fpsy.2010.00150
- 9 54. Stefansson H, Helgason A, Thorleifsson G, et al. A common inversion under selection
10 in Europeans. *Nat Genet.* 2005;37(2):129-137. doi:10.1038/ng1508
- 11 55. Zody MC, Jiang Z, Fung HC, et al. Evolutionary toggling of the MAPT 17q21.31
12 inversion region. *Nat Genet.* 2008;40(9):1076-1083. doi:10.1038/ng.193
- 13 56. Pittman AM, Myers AJ, Abou-Sleiman P, et al. Linkage disequilibrium fine mapping
14 and haplotype association analysis of the tau gene in progressive supranuclear palsy
15 and corticobasal degeneration. *J Med Genet.* 2005;42(11):837-846.
16 doi:10.1136/jmg.2005.031377
- 17 57. Hutton M, Lendon CL, Rizzu P, et al. Association of missense and 5'-splice-site
18 mutations in tau with the inherited dementia FTDP-17. *Nature.* 1998;393(6686):702-
19 705. doi:10.1038/31508
- 20 58. Healy DG, Abou-Sleiman PM, Lees AJ, et al. Tau gene and Parkinson's disease: a
21 case-control study and meta-analysis. *J Neurol Neurosurg Psychiatry.*
22 2004;75(7):962-965. doi:10.1136/JNNP.2003.026203
- 23 59. Fung H-C, Scholz S, Matarin M, et al. Genome-wide genotyping in Parkinson's
24 disease and neurologically normal controls: first stage analysis and public release of
25 data. *Lancet Neurol.* 2006;5(11):911-916. doi:10.1016/S1474-4422(06)70578-6
- 26 60. Dong X, Liao Z, Gritsch D, et al. Enhancers active in dopamine neurons are a primary
27 link between genetic variation and neuropsychiatric disease. *Nat Neurosci.*
28 2018;21(10):1482-1492. doi:10.1038/s41593-018-0223-0
- 29 61. Ferrari R, Wang Y, Vandrovcova J, et al. Genetic architecture of sporadic
30 frontotemporal dementia and overlap with Alzheimer's and Parkinson's diseases. *J*
31 *Neurol Neurosurg Psychiatry.* 2017;88(2):152-164. doi:10.1136/JNNP-2016-314411

- 1 62. Koks S, Pfaff AL, Bubb VJ, Quinn JP. Transcript Variants of Genes Involved in
2 Neurodegeneration Are Differentially Regulated by the APOE and MAPT Haplotypes.
3 *Genes* 2021, Vol 12, Page 423. 2021;12(3):423. doi:10.3390/GENES12030423
- 4 63. Soto-Beasley AI, Walton RL, Valentino RR, et al. Screening non-MAPT genes of the
5 Chr17q21 H1 haplotype in Parkinson's disease. *Parkinsonism Relat Disord*.
6 2020;78:138-144. doi:10.1016/J.PARKRELDIS.2020.07.022
- 7 64. Swatek KN, Komander D. Ubiquitin modifications. *Cell Res*. 2016;26(4):399-422.
8 doi:10.1038/cr.2016.39
- 9 65. Koolen DA, Pfundt R, Linda K, et al. The Koolen-de Vries syndrome: a phenotypic
10 comparison of patients with a 17q21.31 microdeletion versus a KANSL1 sequence
11 variant. *Eur J Hum Genet* 2016 245. 2015;24(5):652-659. doi:10.1038/ejhg.2015.178
- 12 66. Li L, Ghorbani M, Weisz-Hubshman M, et al. Lysine acetyltransferase 8 is involved in
13 cerebral development and syndromic intellectual disability. *J Clin Invest*.
14 2020;130(3):1431-1445. doi:10.1172/JCI131145
- 15 67. Valente EM, Abou-Sleiman PM, Caputo V, et al. Hereditary early-onset Parkinson's
16 disease caused by mutations in PINK1. *Science* (80-). 2004;304(5674):1158-1160.
17 doi:10.1126/science.1096284
- 18 68. Kitada T, Asakawa S, Hattori N, et al. Mutations in the parkin gene cause autosomal
19 recessive juvenile parkinsonism. *Nature*. 1998;392(6676):605-608. doi:10.1038/33416
- 20 69. Chu CT. Mechanisms of selective autophagy and mitophagy: Implications for
21 neurodegenerative diseases. *Neurobiol Dis*. 2019;122(July 2018):23-34.
22 doi:10.1016/j.nbd.2018.07.015
- 23 70. Lek M, Karczewski KJ, Minikel E V, et al. Analysis of protein-coding genetic
24 variation in 60,706 humans. *Nature*. 2016;536(7616):285-291.
25 doi:10.1038/nature19057

26

27

1 **FIGURE LEGENDS**

2 **Figure 1 High content mitophagy screen of PD risk genes identifies KAT8 as a**
3 **modulator of pUb(Ser65) levels. A.** Workflow of the high content screen for O/A-induced
4 pUb(Ser65) levels. **B.** pUb(Ser65) Z-scores of one representative mitophagy screen plate. **C.**
5 Overview of the PD GWAS genetic signal at the *KAT8* locus. **D.** Representative **IB** of
6 mitochondrial fractions from SCR, PINK1 and KAT8 KD POE SHSY5Y treated with 1 μ M
7 O/A for 1.5 or 3 h. **E.** Quantification of pUb(Ser65) in E (n=5, one-way ANOVA with
8 Dunnett's correction). **F.** Quantification of PINK1 in E (n=4, one-way ANOVA with
9 Dunnett's correction). **G.** Quantification of KAT8 in E (n=5, one-way ANOVA with
10 Dunnett's correction). **H.** pUb(Ser65) Z-scores of one representative KAT screen plate. See
11 Supplementary Table 5 for the complete list of the genes screened. Data are shown as mean \pm
12 SD.

13
14 **Figure 2 Knockdown of KANSL1 affects pUb(Ser65) levels. A.** Quantification of
15 pUb(Ser65) following treatment of SCR, PINK1 or NSL components siRNA KD POE
16 SHSY5Y cells with 1 μ M O/A for 1.5 h. Data are shown as mean \pm SD; n=6, one-way
17 ANOVA with Dunnett's correction. **B.** Representative images of pUb(Ser65) (green)
18 following treatment of SCR, PINK1 and KANSL1 KD POE SHSY5Y cells with 1 μ M O/A
19 for 3 h. Insets show the nuclei (blue) for the same fields. Scale bar = 20 μ m. **C.**
20 Quantification of pUb(Ser65) in B (n=3, two-way ANOVA with Dunnett's correction). **D.**
21 Representative **IB** of mitochondrial fractions from SCR, PINK1 and KANSL1 KD POE
22 SHSY5Y treated with 1 μ M O/A for 1.5 or 3 h. **E.** Quantification of pUb(Ser65) in D (n=5,
23 one-way ANOVA with Dunnett's correction). **F.** Quantification of PINK1 in D (n=4, one-
24 way ANOVA with Dunnett's correction). Data are shown as mean \pm SD.

25
26 **Figure 3 KAT8 and KANSL1 knockdown decreases PINK1-dependent mitophagy**
27 **initiation. A.** Representative images of pUb(Ser65) (green) following treatment of SCR,
28 PINK1, KAT8 and KANSL1 KD POE SHSY5Y cells with 1 μ M O/A for 0-7 h. Insets show
29 the nuclei (blue) for the same fields. Scale bar = 20 μ m. **B.** Quantification of pUb(Ser65) in A
30 (n=6, two-way ANOVA with Dunnett's correction). For details on the statistical test, see
31 Supplementary Table 6. **C.** Representative images of FLAG-Parkin (green) with Hoechst
32 nuclei counterstain (blue) following treatment of SCR, PINK1 and KAT8 siRNA KD POE

1 SHSY5Y with 1 μ M O/A for 3 h. Scale bar = 20 μ m. **D.** Quantification of FLAG-Parkin
 2 recruitment to the mitochondria as a ratio of FLAG intensity in the mitochondria and in the
 3 cytosol in C (n=5, two-way ANOVA with Dunnett's correction). **E.** Representative images of
 4 pParkin (green) with Hoechst nuclei counterstain (blue) following treatment of SCR, PINK1
 5 and KAT8 siRNA KD POE SHSY5Y with 1 μ M O/A for 3 h. Scale bar = 20 μ m. **F.**
 6 Quantification of pParkin levels in E (n=5, two-way ANOVA with Dunnett's correction).
 7 Data are shown as mean \pm SD.

8

9 **Figure 4 RT-qPCR Assessments of *KANSL1*, *KAT8*, *PINK1* and *PRKN* gene expression**
 10 **in POE and WT SHSY5Ys. A-C.** RT-qPCR quantification of *KANSL1* mRNA (A), *KAT8*
 11 mRNA (B) and *PINK1* mRNA (C) in POE SHSY5Ys (n=6, one-way ANOVA with
 12 Dunnett's correction). **D-G.** RT-qPCR quantification of *KANSL1* mRNA (D), *KAT8* mRNA
 13 (E), *PINK1* mRNA (F) and *PRKN* mRNA (G) in WT SHSY5Ys (n=5, one-way ANOVA
 14 with Dunnett's correction). Data are shown as mean \pm SD.

15

16 **Figure 5 *KANSL1* and *KAT8* knockdown decrease mitochondrial clearance. A.**
 17 Representative images of mt-Keima following treatment of SCR, PINK1 and KAT8 siRNA
 18 KD POE SHSY5Y with 1 μ M O/A for 0-8 h. The first and third rows show the neutral
 19 Keima-green signal (green) counterstained with Hoechst (blue) after 0 h and 6 h respectively
 20 of DMSO vs O/A. The second and fourth rows show the acidic lysosomal Keima-red signal
 21 (red) counterstained with Hoechst (blue) after 0 h and 6 h respectively of DMSO vs O/A.
 22 Scale bar = 25 μ m. **B.** Quantification of the mitophagy index, calculated as the ratio of the
 23 area of lysosomal mt-Keima signal and total mt-Keima signal in A (n=3, one-way ANOVA
 24 with Dunnett's correction). For details on the statistical test, see Supplementary Table 7. Data
 25 are shown as mean \pm SD.

26

27 **Figure 6 *KANSL1* presents ASE sites in LD with the H1/H2 SNP, and pUb(Ser65) levels**
 28 **are altered by siRNA KD of *KANSL1* but not other genes present at the 17q21 locus. A.**
 29 ASEs derived from putamen and substantia nigra in high linkage disequilibrium with the
 30 H1/H2 tagging SNP, rs12185268 and their position along the *KANSL1* gene. The missense
 31 variants track displays the variants annotated as missense by gnomAD v2.1.1⁷⁰. The valid
 32 track displays the heterozygous sites (orange = missense) with an average read depth greater

1 than 15 reads across all samples, which were examined for ASE. The topmost track displays
2 the FDR-corrected minimum $-\log_{10}$ p-value across samples for the sites that show an ASE in
3 at least one sample. **B.** Conservation of the KANSL1 protein across species. The four coding
4 variants (NM_001193465) in the *KANSL1* gene are in high LD ($r^2 > 0.8$) with the H1/H2
5 haplotypes. **C.** pUb(Ser65) Z-scores of one representative 17q21 locus screen plate. See
6 Supplementary Table 10 for the complete list of the genes screened.

7

8 **Figure 7 pUb(Ser65) levels are reduced in isogenic iNeurons with heterozygous**
9 **KANSL1^{+/-} loss of function and CRISPRi-i3N iNeurons with KANSL1 and KAT8**
10 **sgRNA KD** **A.** Representative IB of isogenic d17 iNeurons with/without heterozygous LoF
11 frameshift mutation in KANSL1 treated with 1 μ M O/A over a 12 h extended time-course. **B.**
12 Quantification of pUb(Ser65) in A (n=4 inductions, two-way ANOVA with Dunnett's
13 correction). **C.** Representative images of pUb(Ser65) (yellow) with Hoechst nuclei
14 counterstain (blue) following treatment of non-transduced (No TD), non-targeting, KANSL1,
15 KAT8 and PINK1 sgRNA KD d17 CRISPRi-i3N iNeurons with 1 μ M O/A vs DMSO for 9
16 h. Inserts show staining for TOM20 (cyan) and mCherry transduction reporter (magenta) with
17 Hoechst nuclei counterstain (blue) for the same field of view. Scale bar = 100 μ m. **D.**
18 Quantification of pUb(Ser65) intensity in TOM20 defined mitochondrial area in D (n=3
19 inductions, two-way ANOVA with Dunnett's correction). Data are shown as mean \pm SD.

20

21

22

1 **Table 1 Overview of bioinformatic evidence for genes prioritised and taken forward for**
 2 **downstream functional analysis**

Gene	CoIB	CoIG	PPI	GWAS	MPD	MLS
ATP13A2					X	X
CCNT2				X		
CD38	X	X		X		
CTSB	X	X	X			
DDRGI1				X		
DGKQ				X		
DJI					X	
DNAJC13					X	
FBXO7					X	
GALC	X			X		X
GBA			X		X	X
GPNMB	X	X		X		
HSD3B7		X				
IDUA						X
INPP5F			X			
KAT8		X	X	X		
KLHL7		X		X		
LRRK2			X	X	X	
LSM7	X	X		X		
MAPT			X	X		
NCKIPSD	X	X	X	X		
NEK1	X					
NSF			X			
NUCKS1		X		X		
NUPL2	X	X		X		
PDLIM2		X		X		
PM20D1	X					
PRKN					X	
RAB7L1	X	X	X			
SH3GL2			X			
SLC41A1		X		X		
SNCA					X	
SPPL2B	X					
STK39				X		
VAMP4	X	X				
VPS35					X	
WDR6	X	X				
ZNF646				X		

3 CoIB = coloc analysis using Braineac; CoIG = coloc analysis using GTEx; GWAS = genes prioritised in PD-GWAS³; MLS = Mendelian
 4 genes associated with lysosomal storage disorders; MPD = Mendelian genes associated with PD; WPPINA = weighted protein interaction
 5 network.

6

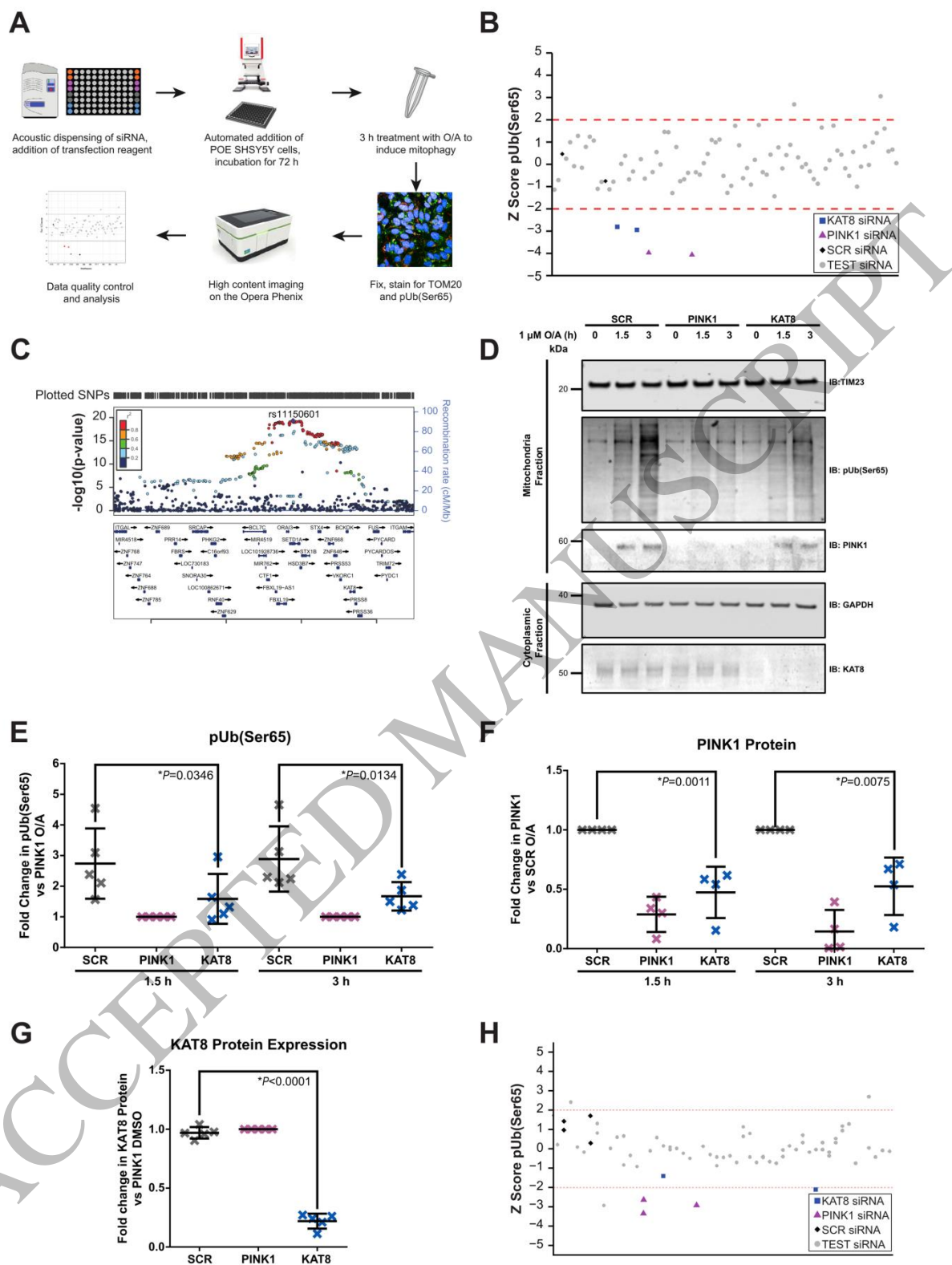


Figure 1
421x559 mm (.59 x DPI)

1
2
3
4

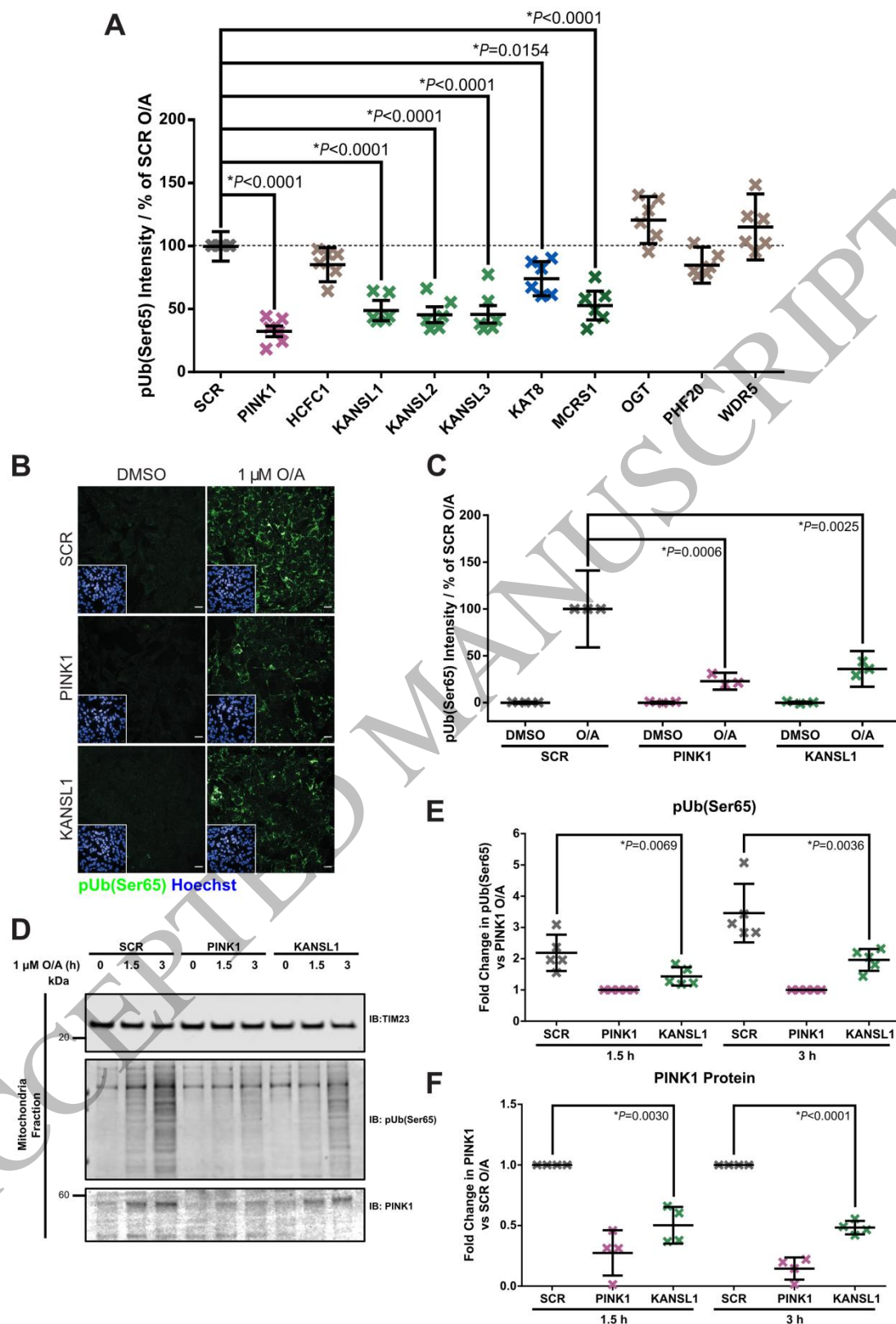


Figure 2
395x559 mm (.59 x DPI)

1
2
3
4

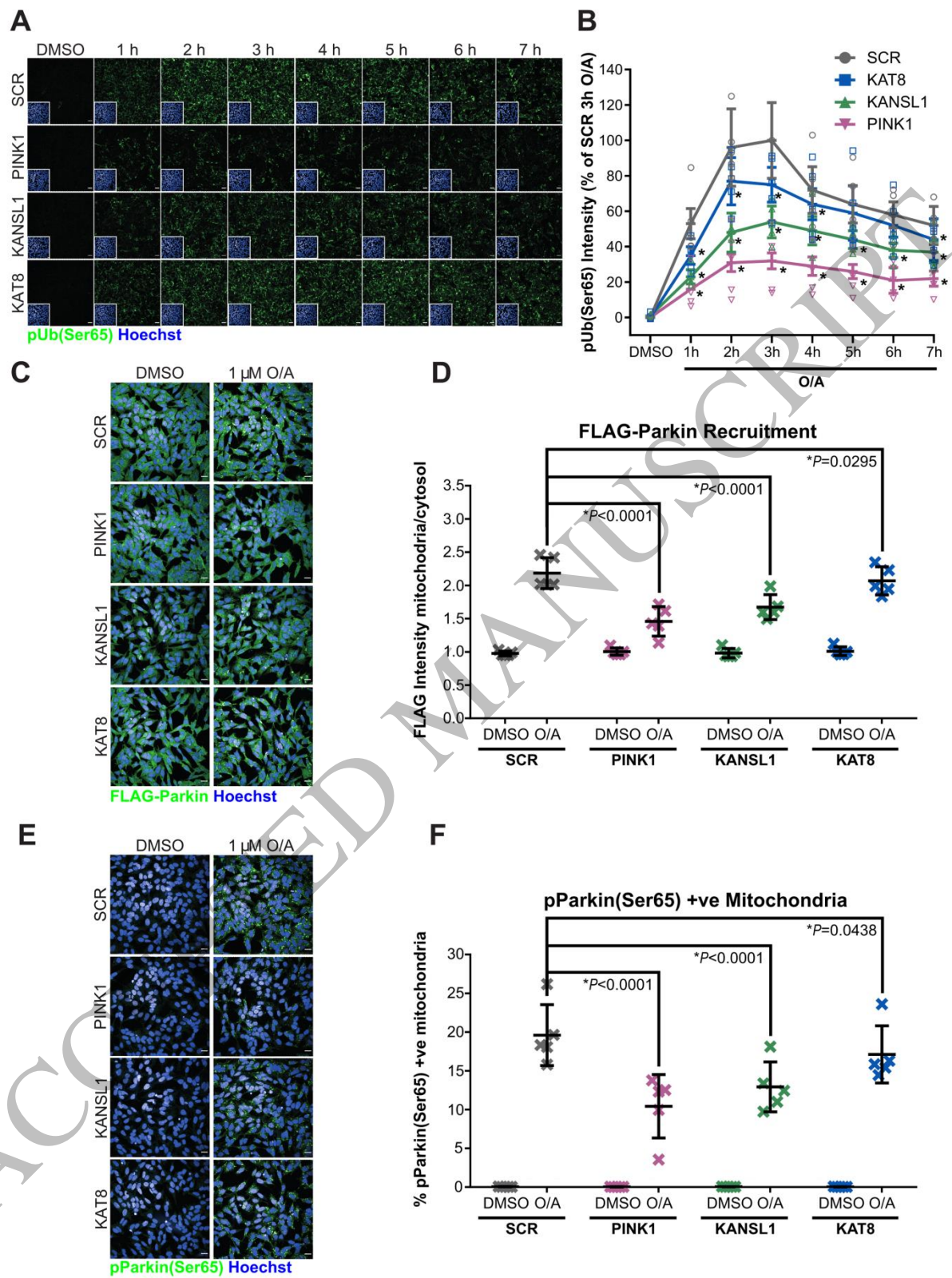


Figure 3
411x559 mm (.59 x DPI)

1
2
3
4

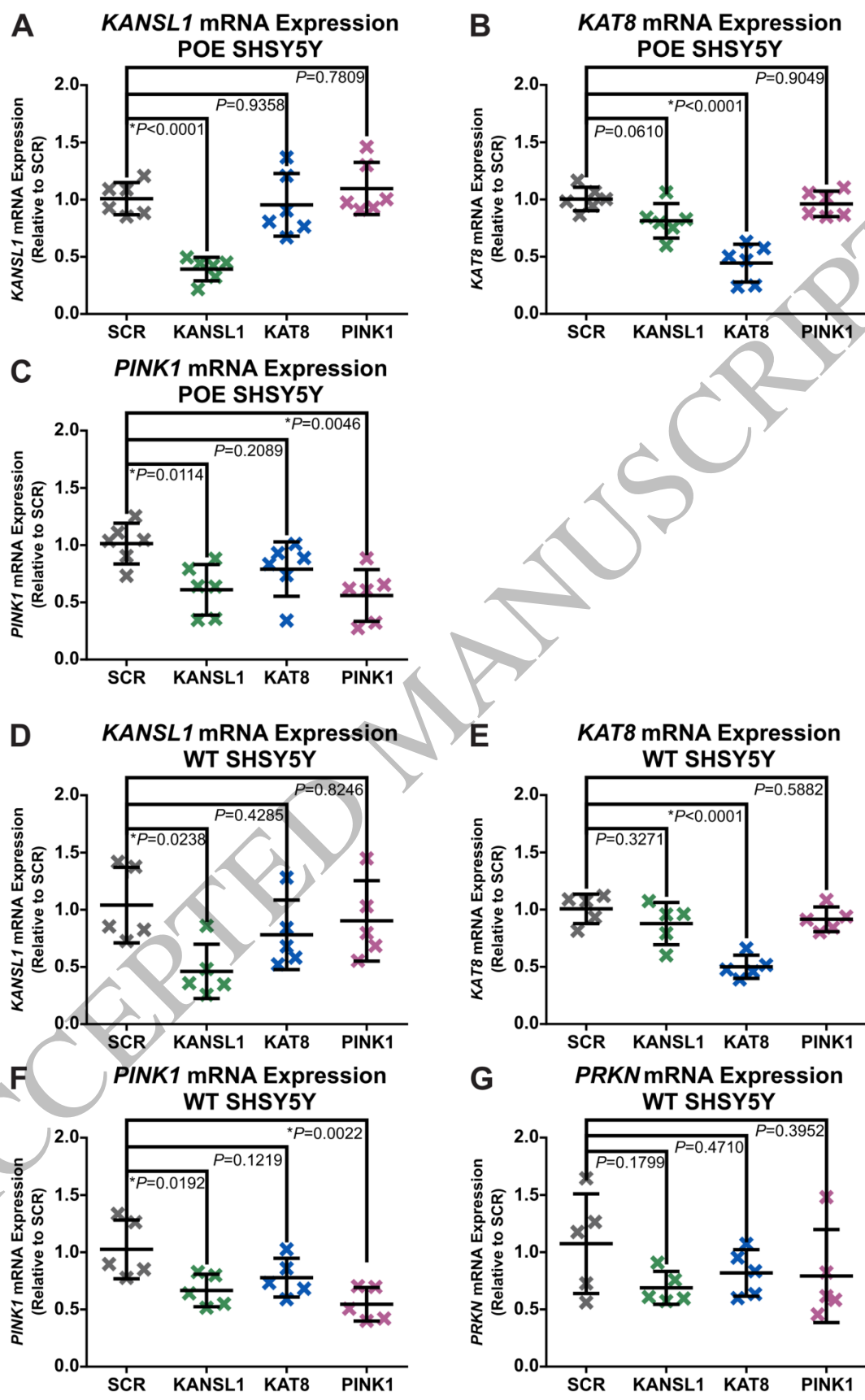


Figure 4
353x559 mm (.59 x DPI)

1
2
3

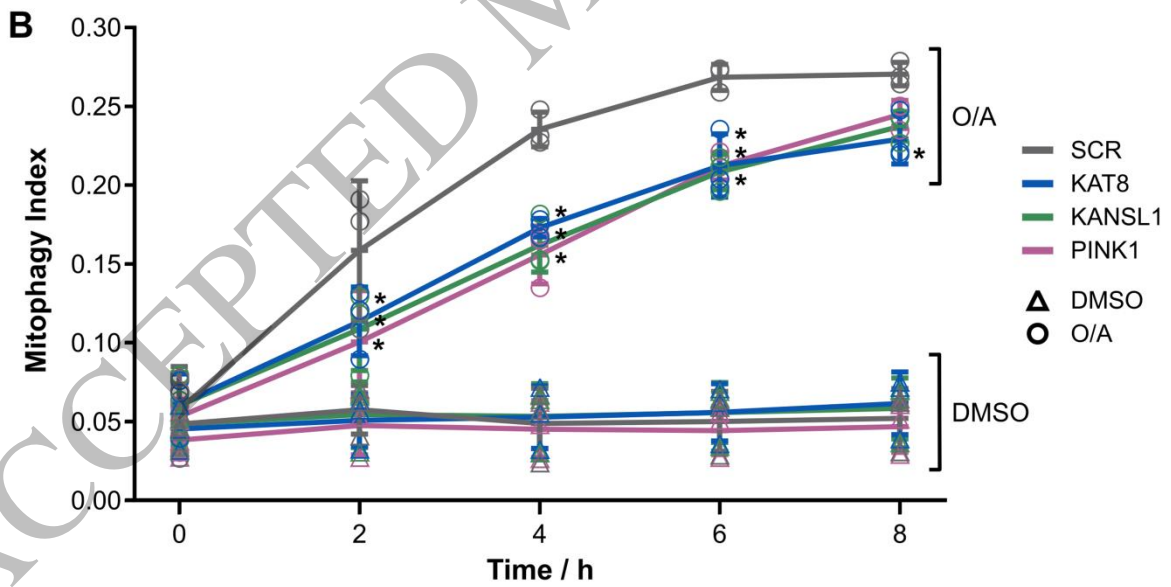
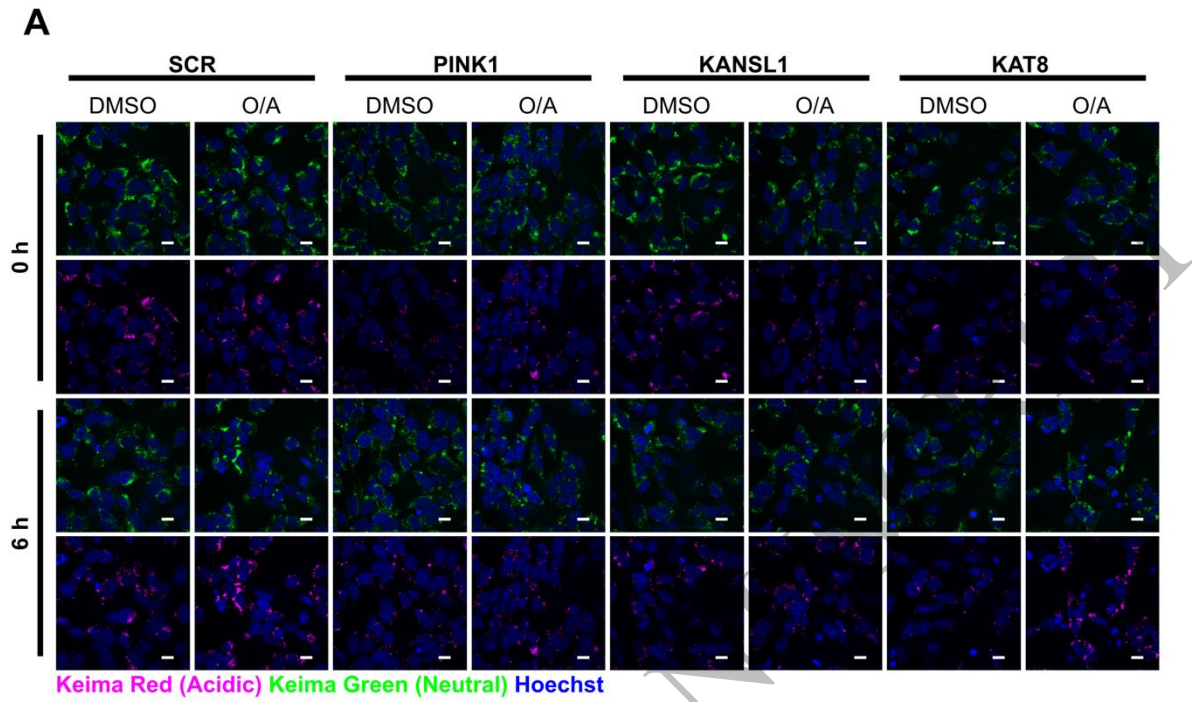


Figure 5
460x559 mm (.59 x DPI)

2
3
4
5

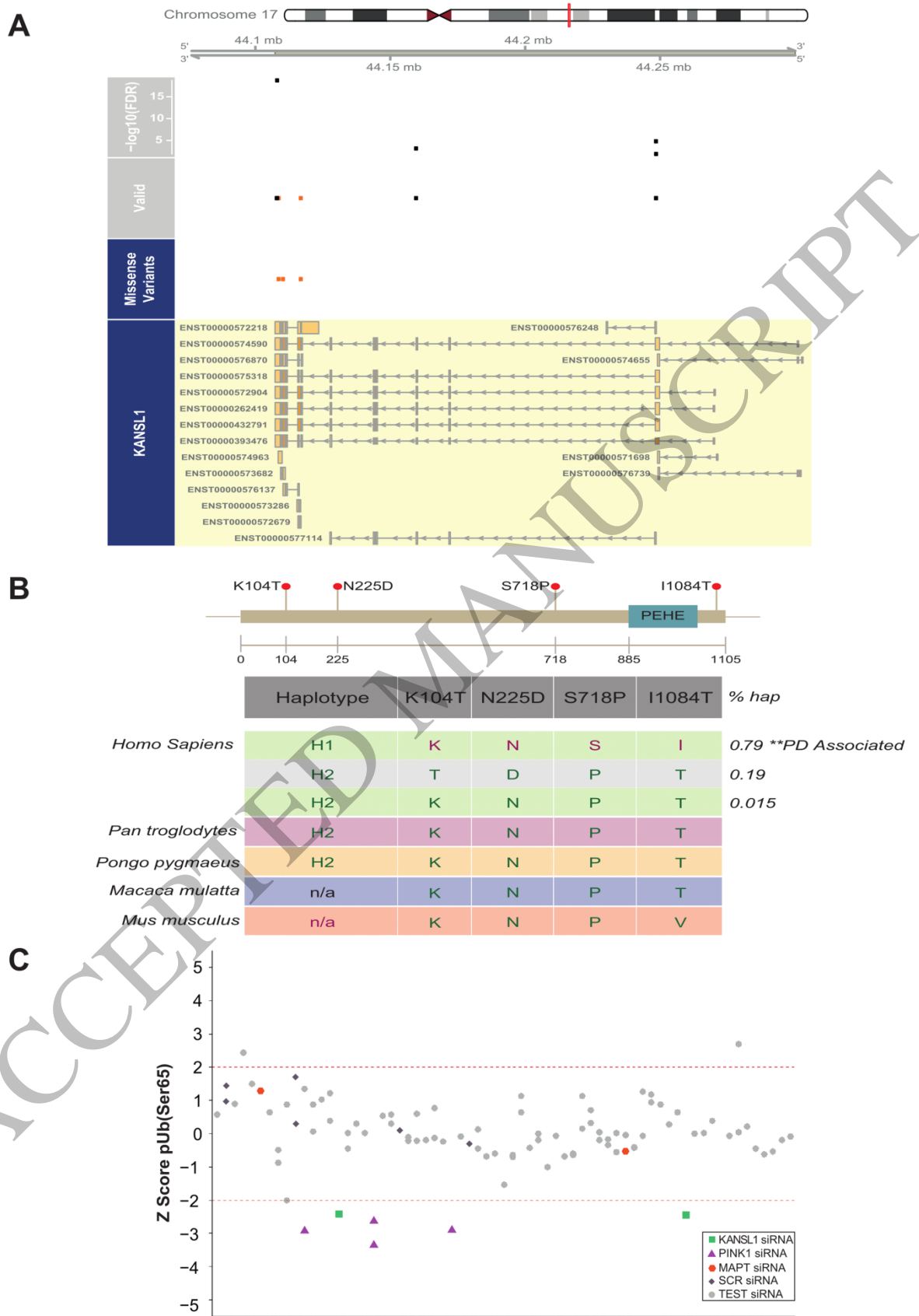


Figure 6
380x559 mm (.59 x DPI)

1
2
3

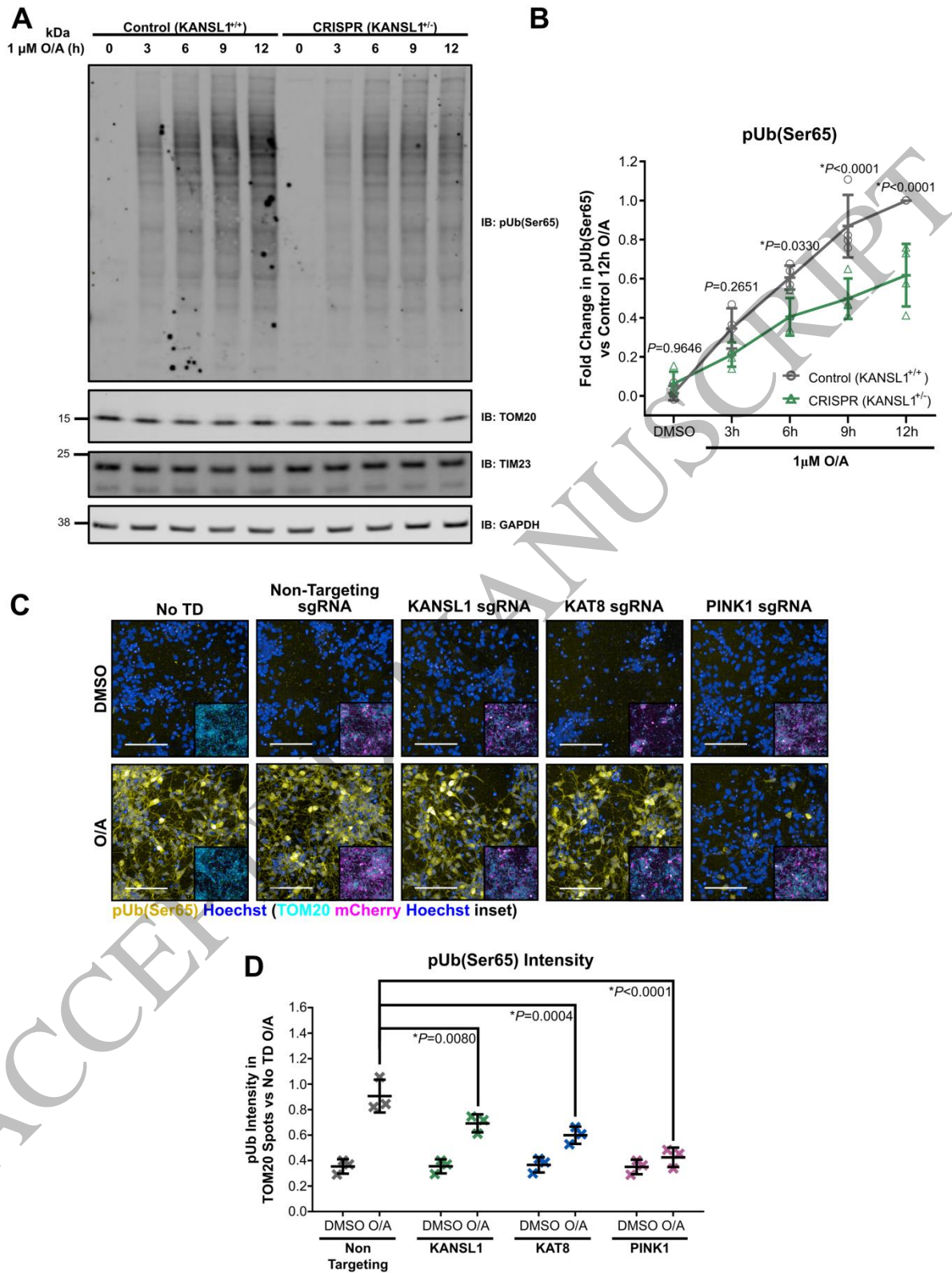


Figure 7
414x559 mm (.59 x DPI)